



Distributed dislocation problems in wedge shaped domains

Daniel J. Riddoch^{*}, David A. Hills

Department of Engineering Science, University of Oxford, Parks Road, OX1 3PJ Oxford, United Kingdom

ARTICLE INFO

Keywords:

Contact mechanics
Cracking
Elasticity
Friction
Stress intensity factors
Dislocations

ABSTRACT

We describe a method to tackle problems such as the presence of cracks or a region of partial slip, in wedge shaped domains, using distributed dislocations, alternatively considered as the edges of complete contacts. An asymptotic solution is sought, which is then applicable to many different contacts. Efficiencies are sought and described in comparison to previous approaches, both in terms of computational cost and kernel complexity. Three example problems, a crack, a slip zone, and a pair of cracks, are discussed.

1. Introduction

Wedge shaped domains arise in practical engineering problems, either in their own right, or when associated with the edge of a complete contact problem, where the contact in its adhered state is considered to be similar to a wedge, whose internal angle is the sum of the angle of contact within the contact defining body and a half plane. The surface tractions are identical on the adhered surfaces, and the interface transmits contact tractions. For this reason it is often of practical importance to determine the state of stress in wedges, and to be able to account for limited violations of continuity, such as the presence of a short crack, or the attainment of limiting friction, in the case of an adhered complete, or sharp-edged, contact.

A common approach to this problem is to use the well known solution of Williams (1952) to describe the state of stress in the wedge. The Williams solution indicates that the stresses at the apex of a reentrant wedge will be singular, and composed of a symmetric(mode I) and anti-symmetric(mode II) component, with other bounded terms in the infinite expansion that is found being dominated by these two terms at the edge of contact. The mode I term will be singular for all reentrant wedges, that is all wedges having total internal angle greater than 180° , where as the dominant mode II term is singular for wedges having total internal angle greater than approximately 257.4° , so one where the contact defining body has an internal angle less than 77.4° .

In practical applications a singular state of stress cannot be sustained, as all realistic materials have a finite yield stress. The state of stress must therefore be relieved. In this analysis we consider methods of relieving this stress by permitting slip. Plasticity might also be present, as has been discussed by previous studies, including by Hills and Dini (2011), but we will not discuss it any further here.

In the absence of plasticity, the singular state of stress may be relieved by either the presence of a crack, or by a zone of partial slip. These phenomena themselves introduce constraints upon the problem. The faces of an open crack must be traction free, and a zone of partial slip must obey a friction law. A method is therefore required which enforces these conditions, and preserves the conditions of the wedge, chiefly that the free surfaces of the wedge be free of tractions, and allows us to calculate the resulting state of stress in the wedge.

Using the Williams solution as a basis, previous work has used a series of distributed dislocations to modify the state of stress to account for the friction law, or the requirement for the faces of an open crack to be traction free (Churchman and Hills, 2006a,b; Riddoch and Hills, 2023a). However, there is a problem with this approach, which arises from the need to know the state of stress caused by the dislocations themselves in the domain under consideration.

The kernels, functions which describe the stress components induced by a dislocation, are well understood for a dislocation placed in an infinite plane. However, no closed form solution exists for dislocations in a wedge, except in special cases, such as a half-plane, which is simply a wedge with total internal angle of 180° . Some method must be devised based on the infinite plane kernels and which does not induce tractions on the free surfaces.

Hecker and Romanov (1992, 1993) proposed a method whereby an object dislocation is placed in an infinite plane, in the same position as the dislocation for which the state of stress is sought. This is referred to as the object dislocation. Then, distributions of dislocations are placed along trace lines which coincide with the free surfaces of the wedge. The density of these distributions is initially held as a variable, and then found using the condition that these lines must be free of traction.

^{*} Corresponding author.

E-mail address: daniel.riddoch@eng.ox.ac.uk (D.J. Riddoch).

That is the influence of the object dislocation, and the distributions of glide and climb edge dislocations on both free surfaces must cancel out exactly on the free surface trace lines. The method does rely on the convergence of the solution, when using a square root singular behaviour rather than true order. The convergence of this has been tested by Churchman et al. (2006) and Yingzhi and Hills (1990).

This method was refined by Churchman et al. (2006) and applied to a three quarter plane, and successfully used to solve the problem of a short crack at the edge of a square contact. Later, Riddoch and Hills (2023b) would generalise this approach using polar coordinates to calculate the kernels at any wedge or interface angle, and use this method to tackle the problem of a crack or pair of cracks at the apex of a wedge (Riddoch and Hills, 2023a), and the problem of a zone of slip at the edge of a contact of arbitrary angle (Riddoch and Hills, 2023c).

2. An alternative approach

In all the examples mentioned so far, the basic approach has been the same as that originally described by Hecker and Romanov, where a kernel is found for an individual dislocation, and then these kernels are used to solve a distributed dislocation problem by superposition. However, in this analysis, we will consider another way. Given that the resultant dislocations are used to solve a distributed dislocation problem, and are themselves found by solving a distributed dislocation problem, and the conditions that both enforce must be simultaneously true for the problem to be solved, we can consider the two problems simultaneously.

As such, consider distributing dislocation along the trace lines representing the free surfaces of the wedge in an infinite plane, and at the same time distributing dislocations along the crack faces or slip region whose effect on the state of stress of the wedge is to be calculated. We once again enforce the conditions that the crack faces be traction free, or that the slip zone follows a friction law, but now we must also consider simultaneously the effect of the dislocations on the free surfaces. We also enforce the conditions that the free surfaces be traction free, considering the effect of the other free surface, and the crack faces or slip interface.

3. A crack at the wedge apex

Let us now consider an example problem. We have already discussed the example of a crack at the edge of a complete contact, or the apex of a wedge. This problem has been solved by Churchman and Hills (2006a) for a three quarter plane, and generalised by Riddoch and Hills (2023a). Both previous studies used the method laid out by Hecker and Romanov, using what we shall now call the sequential method.

Using our new method, we consider the problem of a single crack of length l , placed at an angle ϕ from the bisector of a wedge of total internal angle 2α . We place dislocations along the crack face, and along the free surface trace lines, using \oplus to designate the line with $\theta = \alpha$, and \ominus to denote the line having $\theta = -\alpha$. Fig. 1 shows the layout of this system, which we now refer to as the simultaneous method.

The influence of a dislocation on the state of stress at a remote point is calculated by the product of the Burgers vector and the relevant dislocation kernel function. The influence of a distribution is then calculated by a sum, which can, in practice, be turned into an integral, by converting the Burgers vector's into a dislocation density. This is a contour integral along the line which the dislocations are distributed along. In this example, these contours are straight lines, which in polar coordinates can all be written as $\theta = \psi$, with ψ being some value of angle measured from the bisector of the wedge.

One of the disadvantages of the work of Churchman et al. (2006), is that the dislocation kernels are calculated only along perpendicular lines. One of the consequences of this assumption is that not all distributions of dislocations arise, as glide edge dislocations do not induce any normal stress along the line parallel to their Burgers vector, and climb

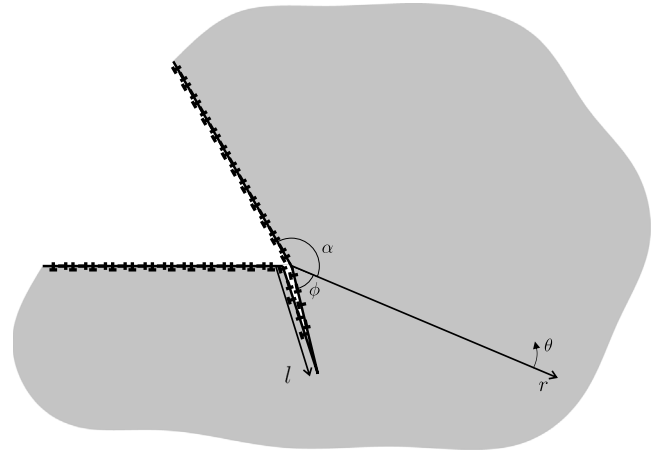


Fig. 1. Sketch of distributed dislocations on free surfaces and crack faces.

edge dislocations do not induce any shear stress on the line parallel to their Burgers vector. However, as part of the motivation for this analysis is the generalisation of the crack and/or contact angles, it is necessary to consider all distributions of dislocations here.

This problem requires six distributions of dislocations along three lines. The free surfaces of the wedge are unable to support tractions. Therefore it is necessary to ensure that no shear or normal traction is induced on these free surfaces, so a distribution of glide edge dislocations is placed on each of the free surfaces lines to remove any induced shear tractions, and a distribution of climb edge dislocations placed similarly to remove any induced normal traction.

In this analysis, a glide edge dislocation will have a Burgers vector b_r , so a distribution of glide edge dislocations is said to have density $B_r(\rho)$, where ρ is the position along the line the dislocations are distributed along, running from the origin of the coordinate system, whose origin is placed at the apex of the wedge. The free surfaces of the wedge correspond to the lines $\theta = \pm\alpha$ in this coordinate system. Therefore, the symbol \oplus is used to denote dislocation densities for those distributions along the line $\theta = \alpha$, and similarly \ominus is used when considering those distributions along the line $\theta = -\alpha$. Hence the density of the two distributions of glide edge dislocations along the free surface lines are represented by $B_r^\oplus(\rho)$ and $B_r^\ominus(\rho)$ for the lines $\theta = \alpha$ and $\theta = -\alpha$ respectively. Similarly, climb edge dislocations have a Burgers vector b_θ , and so the distributions of climb edge dislocations along the free surface lines are represented by $B_\theta^\oplus(\rho)$ and $B_\theta^\ominus(\rho)$ for the lines $\theta = \alpha$ and $\theta = -\alpha$ respectively.

So, the influence on the stress component at a point (r, ψ) , for $r > 0$, and $-\alpha < \psi < \alpha$, of the distributions of dislocations along the free surface line is given by

$$\sigma_{r\theta}(r, \psi) = \frac{2\mu}{\pi(\kappa + 1)} \int_0^\infty B_r^\oplus(\rho) G_{rr\theta}(r, \psi, \rho, \alpha) + B_r^\ominus(\rho) G_{rr\theta}(r, \psi, \rho, -\alpha) + \dots \\ B_r^\ominus(\rho) G_{rr\theta}(r, \psi, \rho, -\alpha) + B_\theta^\oplus(\rho) G_{\theta r\theta}(r, \psi, \rho, \alpha) + \dots \\ B_\theta^\ominus(\rho) G_{\theta r\theta}(r, \psi, \rho, -\alpha) d\rho. \quad (1)$$

The other line along which dislocations must be distributed is the crack line. As we are modelling open cracks, the faces of the crack are free surfaces, and so cannot support any shear or normal traction. The two faces of the crack are treated as a single line, as the opening width of the crack is assumed to be small compared to the crack length. In the same way as we generate the free surfaces, a distribution of glide edge dislocations is placed along the crack line to remove any induced shear traction, the density of this distribution is denoted $B_r(\xi)$, where ξ is the location along the crack line from the origin, note that $\xi \leq l$, the crack length. No superscript is used to specifically identify the crack line. Similarly, a distribution of climb edge dislocations is used to clear any induced normal traction, the density of this distribution is then denoted $B_\theta(\xi)$.

Table 1

Table of boundary conditions.

Line	Normal traction	Shear traction
$\theta = \alpha$	$\sigma_{\theta\theta}(r, \alpha) = 0$ for $r \geq 0$	$\sigma_{r\theta}(r, \alpha) = 0$ for $r \geq 0$
$\theta = -\alpha$	$\sigma_{\theta\theta}(r, -\alpha) = 0$ for $r \geq 0$	$\sigma_{r\theta}(r, -\alpha) = 0$ for $r \geq 0$
$\theta = \phi$	$\sigma_{\theta\theta}(r, \phi) = 0$ for $l \geq r \geq 0$	$\sigma_{r\theta}(r, \phi) = 0$ for $l \geq r \geq 0$

The influence of these distributions of dislocations on a stress component at a point (r, ψ) , for $r > 0$, and $-\alpha < \psi < \alpha$, is then found by

$$\sigma_{r\theta}(r, \psi) = \frac{2\mu}{\pi(\kappa + 1)} \int_0^l B_r(\xi) G_{rr\theta}(r, \psi, \xi, \phi) + B_\theta(\xi) G_{\theta r\theta}(r, \psi, \xi, \phi) d\xi, \quad (2)$$

where l is the crack length, and ϕ is the crack angle.

The combined influence of all of these distributions of dislocations on the state of stress at a point (r, ψ) , for $r > 0$, and $-\alpha < \psi < \alpha$, is then given by

$$\begin{aligned} & \frac{2\mu}{\pi(\kappa + 1)} \int_0^l B_r(\xi) G_{rr\theta}(r, \psi, \xi, \phi) + B_\theta(\xi) G_{\theta r\theta}(r, \psi, \xi, \phi) d\xi + \dots \\ & \frac{2\mu}{\pi(\kappa + 1)} \int_0^\infty B_r^\oplus(\rho) G_{rr\theta}(r, \psi, \rho, \alpha) + B_\theta^\oplus(\rho) G_{\theta r\theta}(r, \psi, \rho, \alpha) + \dots \\ & B_r^\ominus(\rho) G_{rr\theta}(r, \psi, \rho, -\alpha) + B_\theta^\ominus(\rho) G_{\theta r\theta}(r, \psi, \rho, -\alpha) d\rho. \end{aligned} \quad (3)$$

It should be noted that the shear stress component, $\sigma_{r\theta}$ has been used here as an example, and the same procedure can be followed with all stress components, most notably the direct stress $\sigma_{\theta\theta}$.

This influence can then be used to enforce boundary conditions on the free surface lines and the crack line. These have already been mentioned, but are explicitly stated in Table 1. These conditions ensure that the free surfaces are cleared of both shear and normal traction, which they cannot support.

In addition to the stress induced by the placement of dislocations, the enforcement of these boundary conditions also requires a consideration of the tractions induced on these lines by the Williams solution. For the lines $\theta = \pm\alpha$, this is trivial. The boundary conditions of the Williams solution itself requires that the lines be free of tractions, so the tractions implied along them is zero. For the crack line however, this is slightly more complicated, as this line will support stress according to the Williams solution. The tractions along this line are given by

$$\sigma_{r\theta}(r, \phi) = K_I f_{r\theta}^I(\phi) r^{\lambda_I-1} + K_{II} f_{r\theta}^{II}(\phi) r^{\lambda_{II}-1}, \quad (4)$$

$$\sigma_{\theta\theta}(r, \phi) = K_I f_{\theta\theta}^I(\phi) r^{\lambda_I-1} + K_{II} f_{\theta\theta}^{II}(\phi) r^{\lambda_{II}-1}, \quad (5)$$

and these stresses must be added to the influence of the dislocations along the crack line.

The six boundary conditions described in Table 1 can now be enforced. In each case, the sum of the influence of all distributions of dislocations, given for an arbitrary point in Eq. (3), is added to the stress induced by the Williams solution. The conditions state that these six expressions must all equal zero. For the sake of clarity, these equations are reproduced in full in Appendix A, and will not be stated here. However, for illustrative purposes, the equation which enforces the last boundary condition in Table 1, that $\sigma_{r\theta}(r, \phi) = 0$ for $l \geq r \geq 0$, is given by

$$\begin{aligned} & K_I f_{r\theta}^I(\phi) r^{\lambda_I-1} + K_{II} f_{r\theta}^{II}(\phi) r^{\lambda_{II}-1} + \frac{2\mu}{\pi(\kappa + 1)} \int_0^l B_r(\xi) G_{rr\theta}(r, \phi, \xi, \phi) + \dots \\ & B_\theta(\xi) G_{\theta r\theta}(r, \phi, \xi, \phi) d\xi + \frac{2\mu}{\pi(\kappa + 1)} \int_0^\infty B_r^\oplus(\rho) G_{rr\theta}(r, \phi, \rho, \alpha) \\ & + B_\theta^\oplus(\rho) G_{\theta r\theta}(r, \phi, \rho, \alpha) + \dots \\ & B_r^\ominus(\rho) G_{rr\theta}(r, \phi, \rho, -\alpha) + B_\theta^\ominus(\rho) G_{\theta r\theta}(r, \phi, \rho, -\alpha) d\rho = 0, \end{aligned} \quad (6)$$

for $0 \leq r \leq l$.

It can be observed that Eq. (6) contains six unknown functions. These are the six dislocation densities; $B_r, B_\theta, B_r^\oplus, B_\theta^\oplus, B_r^\ominus$, and B_θ^\ominus . It

should also be noted that the functions G_{ijk} contain singular behaviour, so Eq. (6) is a singular integral equation. In order to solve singular integral equations like this, it is necessary to discretise the integrals. In this case, the number of points used to discretise the equations will be decided later, but we can denote the number of points used to discretise the integral along the crack line as n , and the number of points used to discretise the integral along the free surface lines as N .

This discretisation is done using the Gauss–Chebyshev quadratures, described by Erdogan et al. (1973). This is a long winded process, and is once again described in full in Appendix A. One of the requirements of this quadrature is that the end point behaviour is known *a priori*, and it is then isolated and treated separately. This is done by splitting the unknown function, for example B_r , into a pointwise product of two functions, a known function which captures the end point behaviour and singularity and is known as the fundamental function, and an unknown function, denoted ϕ , which is well behaved.

The choice of end point behaviour is either square root singular or square root bounded. This is necessarily an approximation, as the end point behaviour of the unknown functions will not perfectly match this. Previous studies (Churchman et al., 2006; Riddoch and Hills, 2023b) have shown that a sufficient simplification is to think of these options as simply singular or bounded. The choice of end point behaviour must be made with careful consideration of the form of the expected state of stress along each line.

Considering, first, the four distributions along the free surfaces, at the wedge apex, the induced state of stress will be singular in nature. Therefore the density of dislocations required to clear this stress will also be singular. Similarly, at the remote end, the state of stress will be bounded, so the density of dislocations must be bounded. The quadrature also requires the integral to be transformed to the interval $[-1, 1]$, as the integral for the free surface distribution is semi infinite, this requires a Mellin transform, which is laid out in Appendix A. This transform translates the wedge apex to the -1 end of the interval, and the choice of quadrature is described as singular-bounded.

Then considering the distributions along the crack line, these dislocations are treated similarly, so the distribution of dislocations at the wedge apex must be singular, and bounded at the crack tip. As this is a finite interval, a linear transform is used, again set out in Appendix A. This transform translates the crack tip to the -1 end of the interval, so the choice of quadrature is described as bounded-singular. The fundamental functions, weight functions and formula for distribution of points are in all cases given by Hills et al. (2013).

The result of this discretisation is that Eq. (6) becomes a set of n equations in $2n + 4N$ unknowns. Similar discretisation of the equations resulting from the other boundary conditions gives a set of $2n + 4N$ equations in $2n + 4N$ unknowns, which can then be solved simultaneously. The solution to this set of simultaneous equations can then be used to solve the integral equations, and so to find the six unknown functions; $B_r, B_\theta, B_r^\oplus, B_\theta^\oplus, B_r^\ominus$, and B_θ^\ominus .

3.1. Comparison of results

Turning now to a comparison of the results found with either method, firstly, let us compare the calibration matrix which relates the crack tip stress intensity factors K_I^c, K_{II}^c , to the wedge stress intensity factors K_I, K_{II} . This is for a single crack placed at an angle $\frac{\pi}{4}$, in a wedge of half angle $\alpha = \frac{3\pi}{4}$.

Using the sequential method, Riddoch and Hills (2023a) found that

$$\frac{1}{\sqrt{\pi l}} \begin{bmatrix} K_I^c \\ K_{II}^c \end{bmatrix} = \begin{bmatrix} 1.4928 & 1.0894 \\ 0.6070 & -0.3709 \end{bmatrix} \begin{bmatrix} K_I l^{\lambda_I-1} \\ K_{II} l^{\lambda_{II}-1} \end{bmatrix}. \quad (7)$$

whereas using the simultaneous method we find that

$$\frac{1}{\sqrt{\pi l}} \begin{bmatrix} K_I^c \\ K_{II}^c \end{bmatrix} = \begin{bmatrix} 1.4913 & 1.0892 \\ 0.6122 & -0.3713 \end{bmatrix} \begin{bmatrix} K_I l^{\lambda_I-1} \\ K_{II} l^{\lambda_{II}-1} \end{bmatrix}. \quad (8)$$

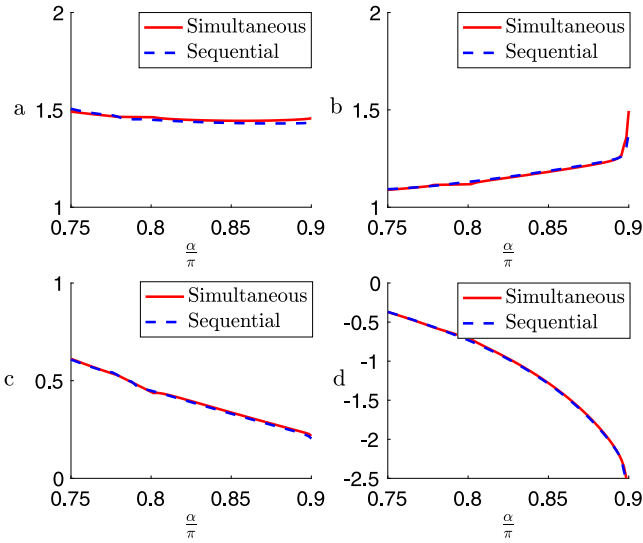


Fig. 2. Plot comparing the calibration matrix coefficients found by both methods for $\frac{3\pi}{4} \leq \alpha \leq \frac{9\pi}{10}$.

These results are very slightly different. However, no element is more than 0.16% different from its previous value, which is well within the margin of error that may be attributed to rounding errors. This is also highlighted in Fig. 2 which shows a comparison of all entries in the calibration matrix for a varying value of α between the three quarter plane $\alpha = 0.75\pi$, and nearer to a full plane $\alpha = 0.9\pi$. It can easily be seen that the values of these coefficients are very similar and well within the margin of error that may be expected when comparing two numerically calculated results.

4. A slip zone at the contact edge

Now we turn our attention to the other problem which we have been discussing. We consider the presence of a zone of partial slip originating from the edge of contact. Previous studies (Riddoch and Hills, 2020; Hills and Dini, 2004) have indicated that the contact is likely to slip outwards under most loading scenarios. Hills and Dini (2004) have also found a bound on the existence of a slip zone, based on the eigenvector ratio at the contact edge.

The Williams solution can also imply the existence of a slip zone, and give an initial guess at to the size of the slip zone. This is the point where $-f_c \sigma_{\theta\theta} = \sigma_{r\theta}$, from the Coulomb friction law, where f_c is the coefficient of friction. The Williams solution indicates that this point, which we denote as c_0 is given by

$$c_0 = \left(-\frac{(f_c - g_{r\theta}^I)K_{II}^o}{(f_c - g_{r\theta}^{II})K_{II}^o} \right)^{\frac{1}{\lambda_{II} - \lambda_I}}, \quad \text{therefore} \quad (9)$$

$$\frac{c_0}{d_0} = \left(-\frac{f_c - g_{r\theta}^I}{f_c - g_{r\theta}^{II}} \right)^{\frac{1}{\lambda_{II} - \lambda_I}}, \quad (10)$$

where $g_{r\theta}^I = \frac{f_{r\theta}^I(\phi)}{f_{\theta\theta}^I(\phi)}$, and $g_{r\theta}^{II} = \frac{f_{r\theta}^{II}(\phi)}{f_{\theta\theta}^{II}(\phi)}$, are the eigenvector ratios, and ϕ is the angle of the contact interface relative to the bisector of the wedge created by combining the two contacting bodies. Note that this is not the true size of the slip, merely an estimate, and we denote the true size of the slip zone c .

As was done for the crack problem, the state of stress can be modified using dislocations to enforce the friction law. This must be done in a way that does not introduce tractions on the free surfaces. Once again, this can be written as a set of boundary conditions, in this case there are five given by

- BC1 The positive free surface line is free of shear stress, $\sigma_{r\theta}(r, \alpha) = 0$, for $r \geq 0$.
- BC2 The positive free surface line is free of normal stress, $\sigma_{\theta\theta}(r, \alpha) = 0$, for $r \geq 0$.
- BC3 The negative free surface line is free of shear stress, $\sigma_{r\theta}(r, -\alpha) = 0$, for $r \geq 0$.
- BC4 The negative free surface line is free of normal stress, $\sigma_{\theta\theta}(r, -\alpha) = 0$, for $r \geq 0$.
- BC5 The friction law is satisfied in the slip region along the contact interface, $-f_c \sigma_{\theta\theta}(r, \phi) = \sigma_{r\theta}(r, \phi)$, for $c \geq r \geq 0$.

In order to enforce these boundary conditions, it is once again necessary to place distributions of glide and climb edge dislocations along the free surfaces. This is done in exactly the same way as for the crack problem described above, and the same notation is used throughout, so the explanation will not be repeated here.

However, along the slip interface, it is only necessary to distribute glide edge dislocations, as the slipping interface can support normal(compressive) traction. This distribution is placed in the slip region, from the corner of the contact, to the slip stick boundary, denoted c . The density of this distribution of glide dislocations is denoted by \bar{B} , in order to avoid confusion with the crack problem. The influence of this distribution of dislocations is found in exactly the same way as was done for the other distributions of dislocations.

The state of stress induced at a point (r, ψ) , for $r > 0$, $-\alpha < \psi < \alpha$, by these dislocations is then found by

$$\begin{aligned} & \frac{2\mu}{\pi(\kappa+1)} \int_0^c \bar{B}(\xi) G_{rr\theta}(r, \psi, \xi, \phi) d\xi + \dots \\ & \frac{2\mu}{\pi(\kappa+1)} \int_0^\infty B_r^\oplus(\rho) G_{rr\theta}(r, \psi, \rho, \alpha) + B_\theta^\oplus(\rho) G_{\theta r\theta}(r, \psi, \rho, \alpha) + \dots \\ & B_r^\ominus(\rho) G_{rr\theta}(r, \psi, \rho, -\alpha) + B_\theta^\ominus(\rho) G_{\theta r\theta}(r, \psi, \rho, -\alpha) d\rho. \end{aligned} \quad (11)$$

Considering also the stress described by the Williams solution, and the state of stress along the contact interface can be described by

$$\begin{aligned} \sigma_{r\theta}(r, \phi) = & K_I f_{r\theta}^I(\phi) + K_{II} f_{r\theta}^{II}(\phi) + \frac{2\mu}{\pi(\kappa+1)} \int_0^c \bar{B}(\xi) G_{rr\theta}(r, \phi, \xi, \phi) d\xi + \dots \\ & \frac{2\mu}{\pi(\kappa+1)} \int_0^\infty B_r^\oplus(\rho) G_{rr\theta}(r, \phi, \rho, \alpha) + B_\theta^\oplus(\rho) G_{\theta r\theta}(r, \phi, \rho, \alpha) + \dots \\ & B_r^\ominus(\rho) G_{rr\theta}(r, \phi, \rho, -\alpha) + B_\theta^\ominus(\rho) G_{\theta r\theta}(r, \phi, \rho, -\alpha) d\rho, \end{aligned} \quad (12)$$

$$\begin{aligned} \sigma_{\theta\theta}(r, \phi) = & K_I f_{\theta\theta}^I(\phi) + K_{II} f_{\theta\theta}^{II}(\phi) + \frac{2\mu}{\pi(\kappa+1)} \int_0^c \bar{B}(\xi) G_{\theta\theta}(r, \phi, \xi, \phi) d\xi + \dots \\ & \frac{2\mu}{\pi(\kappa+1)} \int_0^\infty B_r^\oplus(\rho) G_{\theta\theta}(r, \phi, \rho, \alpha) + B_\theta^\oplus(\rho) G_{\theta\theta}(r, \phi, \rho, \alpha) + \dots \\ & B_r^\ominus(\rho) G_{\theta\theta}(r, \phi, \rho, -\alpha) + B_\theta^\ominus(\rho) G_{\theta\theta}(r, \phi, \rho, -\alpha) d\rho. \end{aligned} \quad (13)$$

Using BC5, the enforcement of the friction law, the formulae given in Eqs. (12) and (13) are then substituted to give the equation

$$\begin{aligned} 0 = & (f_c f_{\theta\theta}^I(\theta) + f_{r\theta}^I(\theta)) K_I r^{\lambda_I - 1} + (f_c f_{\theta\theta}^{II}(\theta) + f_{r\theta}^{II}(\theta)) K_{II} r^{\lambda_{II} - 1} \\ & + \int_0^c \bar{B}(\xi) [f_c G_{r\theta\theta}(r, \phi, \xi, \phi) + \dots \\ & G_{rr\theta}(r, \phi, \xi, \phi)] d\xi + \int_0^\infty f_c [B_r^\oplus(\rho) G_{r\theta\theta}(r, \phi, \rho, \alpha) \\ & + B_\theta^\oplus(\rho) G_{\theta\theta}(r, \phi, \rho, \alpha) + \dots \\ & B_r^\ominus(\rho) G_{r\theta\theta}(r, \phi, \rho, -\alpha) + B_\theta^\ominus(\rho) G_{\theta\theta}(r, \phi, \rho, -\alpha)] + B_r^\oplus(\rho) G_{rr\theta}(r, \phi, \rho, \alpha) + \dots \\ & B_\theta^\oplus(\rho) G_{\theta r\theta}(r, \phi, \rho, \alpha) + B_r^\ominus(\rho) G_{rr\theta}(r, \phi, \rho, -\alpha) + B_\theta^\ominus(\rho) G_{\theta r\theta}(r, \phi, \rho, -\alpha) d\rho \\ & \text{for } 0 \leq r \leq c, \end{aligned} \quad (14)$$

which is a singular integral equation.

The enforcement of the other four boundary conditions is done in the same way and leads to four more singular integral equations. For the sake of clarity, these are reproduced in full in Appendix B, and are not reproduced here.

Once again, the similarity to the crack problem described above is clear. Eq. (14) is a singular integral equation with five unknown

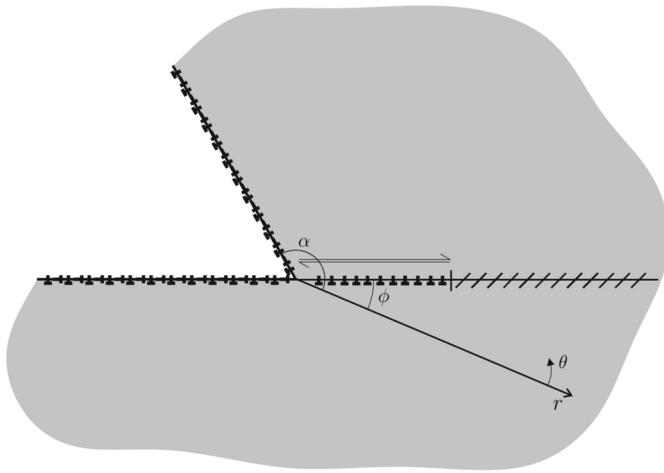


Fig. 3. Sketch of distributed dislocations on free surfaces and slip interface.

functions; \bar{B} , B_r^\oplus , B_θ^\oplus , B_r^\ominus , and B_θ^\ominus . This equation is again discretised, using n points within the slip region, and N points along the free surfaces. These distributions of dislocations are sketched in Fig. 3.

Also, this discretisation is done using the Gauss–Chebyshev quadrature, which requires a choice of fundamental function based on end point behaviour, and a transformation of the integral range to the interval $[-1, 1]$. Once again, a Mellin transform is used for the free surface dislocations, and the singular-bounded quadrature is chosen, the reasons for this are explained above. The choice of quadrature for the slip problem is a little less clear, the behaviour at the slip stick boundary is fairly clear, this must be bounded, as the corrective term created by the influence of the dislocations is correcting a finite value to another finite value.

The behaviour at the contact corner is less clear, as the corrective term must change the state of stress from one singular behaviour to another. This choice was investigated thoroughly by Riddoch and Hills (2023a,b,c), and their conclusion was that the bounded–bounded quadrature is the correct choice, although choosing singular behaviour was shown to not significantly affect the results. The slip region is finite, and so a finite transformation is used in both cases.

This discretisation results in Eq. (14) becoming a set of n equations in $n + 4N$ unknowns. Similar discretisation of the integral equations arising from enforcing the other four boundary conditions results in a set of $n + 4N$ equations in $n + 4N$ unknowns, which can be solved simultaneously and the results used to calculate the value of the unknown functions; \bar{B} , B_r^\oplus , B_θ^\oplus , B_r^\ominus , and B_θ^\ominus .

A complication presented by this problem is the choice of the size of the slip zone. This must be chosen before the equations can be discretised and solved, but cannot be directly calculated as it relies on the solution of the same equations. The solution is to guess the size, based on the estimate c_0 , and then check this guess using conditions imposed on the final solution. The process for doing this is explained in more detail, including an explanation and derivation of the conditions used, by Riddoch and Hills (2023a,b,c).

4.1. Convergence

We now consider the problems of convergence. Using either the sequential or simultaneous methods, both the slip interface and the free surfaces are represented by a finite number of discrete points. For the slip interface, n points are used, and for the free surfaces N points are used. Furthermore, the quadrature requires the choice of two sets of points, known as integration and collocation points. The two sets of points are distinct from each other, meaning that there is always a finite, non-zero distance between any integration and any collocation

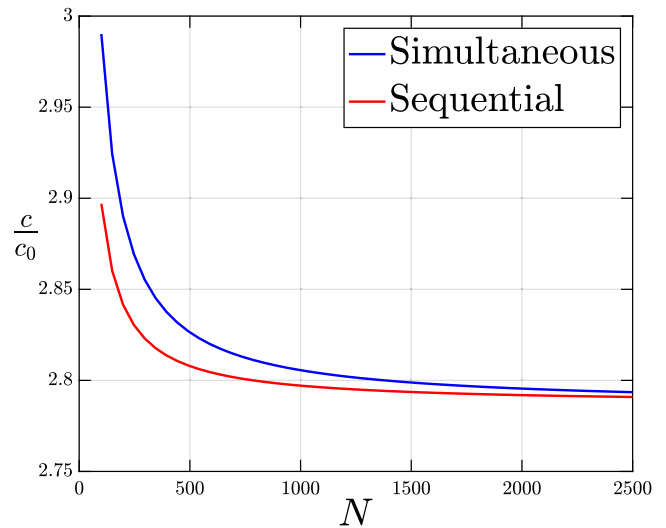


Fig. 4. Variation of calculated slip zone size with number of points used, using both dislocation methods, for a square edged contact with coefficient of friction $f = 0.3$, and remote loading $K_I = -1$, $K_{II} = 1$.

point. This means that any singular, or near singular, behaviour can be described without providing a numerical error, such as requiring division by zero.

According to the choice of end point behaviour, the quadrature describes the distribution of integration and collocation points along the interval $[-1, 1]$. Along the slip interface, a finite transform is used to transform the integration range from $[0, c]$ to $[-1, 1]$, and each of the integration and collocation points can be transformed individually. Along the free surfaces, a Mellin transform is used to transform the range from $[0, \infty)$ to $[-1, 1]$. A log based transform was chosen for this, to simplify the differentiation required during discretisation, but other forms of transform, such as \tan or reciprocal transforms could be used.

The discretisations are necessary for the solution method, but as they represent a discretisation of a truly continuous function, a larger number of points should always give a slightly more accurate result. However, for practical reasons, the greater the number of points the more demanding and therefore the slower the calculation.

So we should consider how many points are necessary. To do this we perform a convergence test, and we will do this for both the sequential and simultaneous methods. We choose two values, N and n , but as these are related, we can infer a ratio between these two. Practical experience has shown that if the number of points on the free surface is five times that on the slip interface, ensuring a similar physical density of points along the slip interface with the choice of transforms, described in Appendix B.

Fig. 4 shows the calculated size of the slip zone changes as the number of points used to calculate changes. It can be seen that a very large number of points is required to guarantee convergence with either method. Computational limitations prevented us from exploring values beyond $N = 2500$, and whilst this proved sufficient to achieve a converged solution using the sequential method, this was not the case for the simultaneous method. This can be determined by the gradient of the lines in Fig. 4.

The distinction made here is quite fine, but is an important one. Fig. 5 shows that the calculated solution changes with coefficient of friction, and that this also affects the convergence of the solution. This highlights the distinction that we have made between a converged and non-converged solution.

It is noteworthy that for this problem, the simultaneous method has not yet converged. This is disappointing and somewhat confusing. However, it is clear that the solution is converging, and it may reasonably

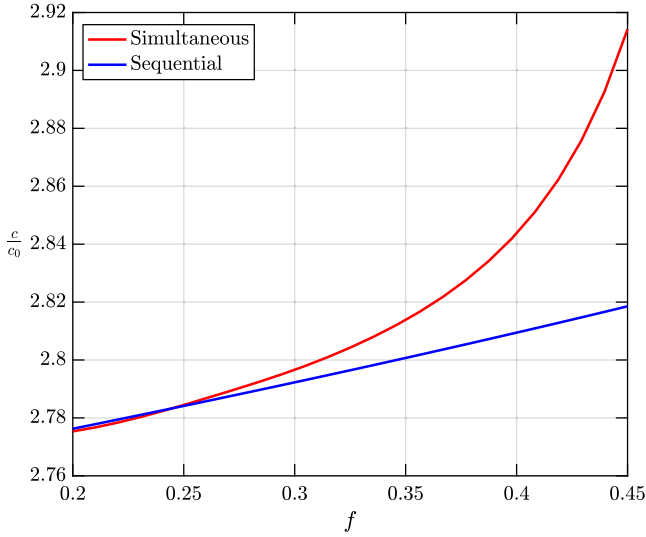


Fig. 5. Overlay plot showing the variation with coefficient of friction of the slip zone size using both dislocation methods.

be expected to converge for some larger value of N . Unfortunately, it is not possible to verify this at this point in time.

5. Two cracks at a wedge apex

Considering again the modelling of crack problems, let us consider the problem of two short straight cracks, whose roots are both at the contact edge/wedge apex. This is a simple development of the single crack problem tackled above, and the same method may be employed. Some modifications will be required to the method and the notation to account for the influence of the second crack, and the effect that may be seen as a result of the two cracks having different lengths.

As before, distributions of glide and climb edge dislocations are placed along the free surfaces, these having densities denoted by; B_r^\oplus for the glide edge dislocations along the line $\theta = \alpha$; B_θ^\oplus for the climb edge dislocations along the line $\theta = \alpha$; B_r^\ominus for the glide edge dislocations along the line $\theta = -\alpha$, and; B_θ^\ominus for the climb edge dislocations along the line $\theta = -\alpha$.

In this case, distributions of dislocations must be placed along both crack faces. To differentiate between the cracks, we number them 1 and 2; the choice of number is not important as long as it is consistent. The number assigned to the crack is used as a subscript or superscript. Distributions of glide and climb edge dislocations, are distributed along the crack faces, their density is denoted; B_r^1 , for the glide dislocations on crack 1, B_θ^1 , for the climb dislocations on crack 1, B_r^2 , for the glide dislocations on crack 2, B_θ^2 , for the climb dislocations on crack 2. This system is sketched in Fig. 6.

The influence of these dislocations can then be calculated in the same way as before, and these can be used to enforce boundary conditions. In this case, as in all cases, the free surfaces cannot support any traction. As in the single crack case, we are modelling the cracks as open cracks, whose faces also cannot support any traction. As such, eight boundary conditions may be enforced. These are laid out in Table 2.

Using the influence functions of the distributions of dislocations, the enforcement of these boundary conditions will give rise to eight simultaneous singular integral equations. As before, these may be discretised using the Gauss–Chebyshev quadratures. Once again a Mellin transform is used to transform the integral range for the distributions along the free surfaces, and a linear transforms is used for the cracks. As for the single crack problem, the singular-bounded quadrature is chosen for the free surfaces and bounded-singular for the cracks.

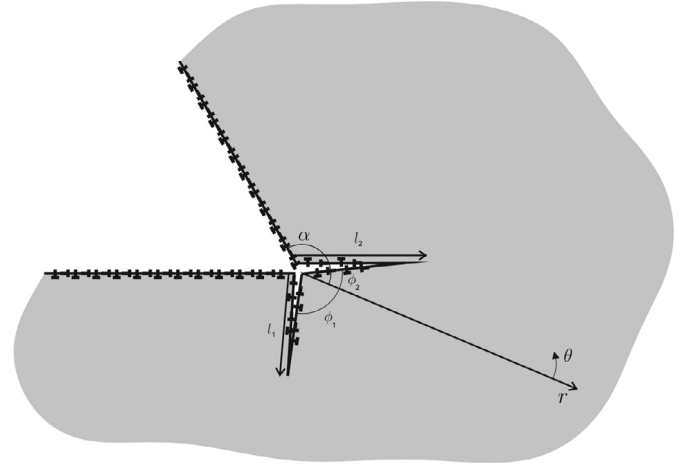


Fig. 6. Sketch of distributed dislocations on free surfaces and crack faces.

Table 2

Table of boundary conditions.

Line	Normal traction	Shear traction
$\theta = \alpha$	$\sigma_{\theta\theta}(r, \alpha) = 0$ for $r \geq 0$	$\sigma_{r\theta}(r, \alpha) = 0$ for $r \geq 0$
$\theta = -\alpha$	$\sigma_{\theta\theta}(r, -\alpha) = 0$ for $r \geq 0$	$\sigma_{r\theta}(r, -\alpha) = 0$ for $r \geq 0$
$\theta = \phi_1$	$\sigma_{\theta\theta}(r, \phi) = 0$ for $l_1 \geq r \geq 0$	$\sigma_{r\theta}(r, \phi) = 0$ for $l_1 \geq r \geq 0$
$\theta = \phi_2$	$\sigma_{\theta\theta}(r, \phi) = 0$ for $l_2 \geq r \geq 0$	$\sigma_{r\theta}(r, \phi) = 0$ for $l_2 \geq r \geq 0$

Table 3

Table comparing the calibration matrices for symmetric cracks in a three quarter plane using different dislocation methods.

Dislocation method	Calibration matrix
Sequential method	$\frac{1}{\sqrt{\pi}} \begin{bmatrix} K_I^1 l_1^{\frac{1}{2}i-1} \\ K_{II}^1 l_1^{\frac{1}{2}ii-1} \\ K_I^2 l_2^{\frac{1}{2}i-1} \\ K_{II}^2 l_2^{\frac{1}{2}ii-1} \end{bmatrix} = \begin{bmatrix} 0.9483 & -1.3765 \\ 0.2459 & 0.1160 \\ 0.9483 & 1.3765 \\ -0.2459 & 0.1160 \end{bmatrix} \begin{bmatrix} K_I \\ K_{II} \end{bmatrix}$
Simultaneous method	$\frac{1}{\sqrt{\pi}} \begin{bmatrix} K_I^1 l_1^{\frac{1}{2}i-1} \\ K_{II}^1 l_1^{\frac{1}{2}ii-1} \\ K_I^2 l_2^{\frac{1}{2}i-1} \\ K_{II}^2 l_2^{\frac{1}{2}ii-1} \end{bmatrix} = \begin{bmatrix} 0.9519 & -1.3768 \\ 0.2502 & 0.1179 \\ 0.9519 & 1.3768 \\ -0.2502 & 0.1179 \end{bmatrix} \begin{bmatrix} K_I \\ K_{II} \end{bmatrix}$

Again as before, this problem has been previously solved using the sequential method by Riddoch and Hills (2023a). Using the simultaneous dislocation method, we are now able to enforce eight conditions, clearing the crack faces and free surfaces of both shear and normal traction. This is detailed in Appendix C. Having these equations, and solving them using MATLAB, we can find the crack tip stress intensity factors related to the wedge stress intensity factors.

5.1. Comparison of results

The stress intensity factors are the primary outputs of the problem, and it is these which we may compare to the results found by Riddoch and Hills (2023a) using the sequential dislocation method. Firstly, let us compare two cracks of equal length. Whilst reviewing the method and results published, an error was found. The correct calibration for a pair of cracks of equal length at right angles to each other and the free surfaces in a three quarter plane, is shown below. Calibrations found with both the simultaneous and sequential methods are shown in Table 3.

Table 4

Table comparing the calibration matrices for a ‘single crack’ in a three quarter plane using different dislocation methods.

Dislocation method	Calibration matrix
Sequential method	$\frac{1}{\sqrt{\pi}} \begin{bmatrix} K_{II}^{1,1} \frac{1}{\sqrt{1-\frac{\alpha}{\pi}}} \\ K_{II}^{1,1} \frac{1}{\sqrt{1-\frac{\alpha}{\pi}}} \\ K_{II}^{2,1} \frac{1}{\sqrt{1-\frac{\alpha}{\pi}}} \\ K_{II}^{2,1} \frac{1}{\sqrt{1-\frac{\alpha}{\pi}}} \end{bmatrix} = \begin{bmatrix} 1.0614 & -1.1759 \\ 0.4941 & 0.3733 \\ N/A & N/A \\ N/A & N/A \end{bmatrix} \begin{bmatrix} K_I \\ K_{II} \end{bmatrix}$
Simultaneous method	$\frac{1}{\sqrt{\pi}} \begin{bmatrix} K_{II}^{1,1} \frac{1}{\sqrt{1-\frac{\alpha}{\pi}}} \\ K_{II}^{1,1} \frac{1}{\sqrt{1-\frac{\alpha}{\pi}}} \\ K_{II}^{2,1} \frac{1}{\sqrt{1-\frac{\alpha}{\pi}}} \\ K_{II}^{2,1} \frac{1}{\sqrt{1-\frac{\alpha}{\pi}}} \end{bmatrix} = \begin{bmatrix} 1.0938 & -1.1901 \\ 0.4416 & 0.4021 \\ N/A & N/A \\ N/A & N/A \end{bmatrix} \begin{bmatrix} K_I \\ K_{II} \end{bmatrix}$

This comparison is encouraging, as although the precise values are not identical, once again the results are well within the margin of error that is expected from numerical calculations. No entry is more than 1.75% different between the two methods.

Alternatively, we may consider the ‘single crack’ problem. This is calculated by making the length of one of the cracks significantly larger than the other, in practice at least 1000 times larger. The effect of the shorter crack is then negligible. The results will not be exactly the same as the results calculated using the single crack model, as the presence of the other crack will have a small effect on the state of stress at the crack root and create a singularity near, but not at the crack root. However, by bringing this singularity, which arises from the tip of the very short crack, nearly to the wedge apex, the effect is reduced. The calibration generated for the shorter crack is useless, as the crack is so short as to be drowned out by noise. Table 4 shows the calibration matrices calculated using both dislocation methods.

Once again these results are encouraging as the calculated results are within the margin of error when compared to each other.

Finally we can now consider the problem of varying the wedge angle. We vary the angle between the three-quarter plane and $\alpha = 0.8\pi$, and Fig. 7 shows how the entries of the calibration matrix compare for cracks of unit and three-quarter unit length respectively, placed at angles $\pi - \alpha$, and $\alpha - \pi$, respectively, so that at the three quarter plane the cracks are perpendicular to each other and the free surfaces and remain perpendicular to each other and the negative free surface throughout.

6. Discussion

Having now considered three example problems, we can consider the efficacy of our new method, as well as discuss some of the advantages and disadvantages presented by the method.

Firstly, let us consider the crack problems. With both the single and two crack problems, close agreement was found between the two dislocation methods. However, there were problems considering the slip problem, which appear to be caused by convergence problems, which are unfortunately unavoidable due to technical limitations of the software used.

This is all well and good, but in all three cases the sequential method developed by Hecker and Romanov (1992, 1993), and applied by Churchman et al. (2006), Churchman and Hills (2006a) and Riddoch and Hills (2023b,a) produced equally good results, and in the slip problem, achieved faster convergence. So we must consider what advantages the simultaneous method described here gives. First among these is computational speed. Experience has shown that this method is significantly faster, by around 20%. This figure is arrived at by comparing the time taken to produce a single graph, like that shown in Fig. 2, the sequential method taking 77.927 s, compared to 63.051 s taken by the simultaneous method. The precise time will obviously vary

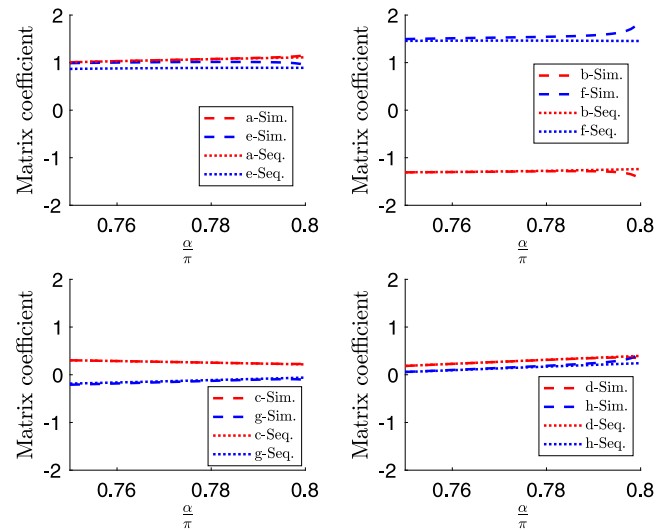


Fig. 7. Plot comparing the calibration matrix coefficients found by both methods for $\frac{3\pi}{4} \leq \alpha \leq \frac{8\pi}{10}$.

depending upon the computer but this is indicative of experience, and the more complex or extensive the problem, the faster the simultaneous method becomes, in relation to the sequential method. This is especially relevant when considering very high resolution problems, using large numbers of points and considering very similar angles each time for example.

The second major advantage is simplicity. This may seem counter-intuitive as the simultaneous method requires fewer integral equations to describe the problem. However, before tackling an example problem the calculation of the stress kernels must be undertaken correctly. This has, of course, been done previously, but to take advantage of this would require the creation and use of a look up table. Furthermore, the only method of verification that the kernel calculations have undergone has been done either by applying the kernels, which may introduce other errors, or by comparison with finite element analysis. By its nature finite element analysis struggles to accurately simulate discontinuities, such as those found at a dislocation core, and the calculation of singularities can lead to errors. The sequential method avoids this problem by using well known and well understood infinite plane kernels, which have been verified over many years of research (Hills et al., 2013; Cottrell et al., 1956).

It should be considered that the simultaneous method has shown problems with convergence for the slip problem, so care must be taken to avoid this issue when considering other problems using this method. Also, the method does generate more integral equations than the simultaneous method, increasing the chance of an error during transcription or discretisation.

7. Conclusion

In this analysis we have developed and explained an alternative dislocation based approach to tackling wedge problems. We have demonstrated that this method has significant advantages in terms of speed and complexity, and does not compromise the fidelity of the results, provided that convergence is guaranteed. We have also explored the convergence of both the sequential and simultaneous methods for the slip and demonstrated why this problem is difficult to solve and prone to errors.

Declaration of competing interest

The authors declare that they have no known competing financial interests or personal relationships that could have appeared to influence the work reported in this paper.

Data availability

Data will be made available on request.

Acknowledgements

Both authors thank Rolls-Royce plc and the EPSRC for the support under the Prosperity Partnership Grant ‘Cornerstone: Mechanical Engineering Science to Enable Aero Propulsion Futures’, Grant Ref: EP/R004951/1.

Appendix A. Single crack integral equations

The single crack problem requires us to enforce six conditions. Clearing the crack face of shear traction, clearing the crack face of normal traction, clearing the positive free surface of shear traction, clearing the positive free surface of normal traction, clearing the negative free surface of shear traction, and finally clearing the negative free surface of normal traction. This gives rise to six integral equations, as described in Section 3. These are given by:

$$\begin{aligned} & -K_{II}f_{r\theta}^I(\phi)r^{\lambda_I-1} - K_{III}f_{r\theta}^{II}(\phi)r^{\lambda_{III}-1} \\ & = \frac{2\mu}{\pi(\kappa+1)} \int_0^l B_r(\xi)G_{rr\theta}(r, \phi, \xi, \phi) d\xi + \dots \\ & B_\theta(\xi)G_{\theta r\theta}(r, \phi, \xi, \phi)d\xi + \frac{2\mu}{\pi(\kappa+1)} \int_0^\infty B_r^\oplus(\rho)G_{rr\theta}(r, \phi, \rho, \alpha) \\ & + B_\theta^\oplus(\rho)G_{\theta r\theta}(r, \phi, \rho, \alpha) d\rho + \dots \\ & B_r^\ominus(\rho)G_{rr\theta}(r, \phi, \rho, -\alpha) + B_\theta^\ominus(\rho)G_{\theta r\theta}(r, \phi, \rho, -\alpha)d\rho, \quad \text{for } 0 \leq r \leq l, \end{aligned} \quad (\text{A.1})$$

$$\begin{aligned} & -K_{II}f_{\theta\theta}^I(\phi)r^{\lambda_I-1} - K_{III}f_{\theta\theta}^{II}(\phi)r^{\lambda_{III}-1} \\ & = \frac{2\mu}{\pi(\kappa+1)} \int_0^l B_r(\xi)G_{r\theta\theta}(r, \phi, \xi, \phi) d\xi + \dots \\ & B_\theta(\xi)G_{\theta\theta\theta}(r, \phi, \xi, \phi)d\xi + \frac{2\mu}{\pi(\kappa+1)} \int_0^\infty B_r^\oplus(\rho)G_{r\theta\theta}(r, \phi, \rho, \alpha) \\ & + B_\theta^\oplus(\rho)G_{\theta\theta\theta}(r, \phi, \rho, \alpha) d\rho + \dots \\ & B_r^\ominus(\rho)G_{r\theta\theta}(r, \phi, \rho, -\alpha) + B_\theta^\ominus(\rho)G_{\theta\theta\theta}(r, \phi, \rho, -\alpha)d\rho, \quad \text{for } 0 \leq r \leq l, \end{aligned} \quad (\text{A.2})$$

$$\begin{aligned} 0 &= \frac{2\mu}{\pi(\kappa+1)} \int_0^c B_r(\xi)G_{rr\theta}(r, \alpha, \xi, \phi) + B_\theta(\xi)G_{\theta r\theta}(r, \alpha, \xi, \phi)d\xi + \dots \\ & \frac{2\mu}{\pi(\kappa+1)} \int_0^\infty B_r^\oplus(\rho)G_{rr\theta}(r, \alpha, \rho, \alpha) + B_\theta^\oplus(\rho)G_{\theta r\theta}(r, \alpha, \rho, \alpha) + \dots \\ & B_r^\ominus(\rho)G_{rr\theta}(r, \alpha, \rho, -\alpha) + B_\theta^\ominus(\rho)G_{\theta r\theta}(r, \alpha, \rho, -\alpha)d\rho \quad \text{for } 0 \leq r \leq \infty, \end{aligned} \quad (\text{A.3})$$

$$\begin{aligned} 0 &= \frac{2\mu}{\pi(\kappa+1)} \int_0^\infty B_r(\xi)G_{r\theta\theta}(r, \alpha, \xi, \phi) + B_\theta(\xi)G_{\theta\theta\theta}(r, \alpha, \xi, \phi)d\xi + \dots \\ & \frac{2\mu}{\pi(\kappa+1)} \int_0^\infty B_r^\oplus(\rho)G_{r\theta\theta}(r, \alpha, \rho, \alpha) + B_\theta^\oplus(\rho)G_{\theta\theta\theta}(r, \alpha, \rho, \alpha) \\ & + B_r^\ominus(\rho)G_{r\theta\theta}(r, \alpha, \rho, -\alpha) + \dots \\ & B_\theta^\ominus(\rho)G_{\theta\theta\theta}(r, \alpha, \rho, -\alpha)d\rho \quad \text{for } 0 \leq r \leq \infty, \end{aligned} \quad (\text{A.4})$$

$$\begin{aligned} 0 &= \frac{2\mu}{\pi(\kappa+1)} \int_0^\infty B_r(\xi)G_{rr\theta}(r, -\alpha, \xi, \phi) + B_\theta(\xi)G_{\theta r\theta}(r, -\alpha, \xi, \phi)d\xi + \dots \\ & \frac{2\mu}{\pi(\kappa+1)} \int_0^\infty B_r^\oplus(\rho)G_{rr\theta}(r, -\alpha, \rho, \alpha) + B_\theta^\oplus(\rho)G_{\theta r\theta}(r, -\alpha, \rho, \alpha) \\ & + B_r^\ominus(\rho)G_{rr\theta}(r, -\alpha, \rho, -\alpha) + \dots \\ & B_\theta^\ominus(\rho)G_{\theta r\theta}(r, -\alpha, \rho, -\alpha)d\rho \quad \text{for } 0 \leq r \leq \infty, \end{aligned} \quad (\text{A.5})$$

$$\begin{aligned} 0 &= \frac{2\mu}{\pi(\kappa+1)} \int_0^\infty B_r(\xi)G_{r\theta\theta}(r, -\alpha, \xi, \phi) + B_\theta(\xi)G_{\theta\theta\theta}(r, -\alpha, \xi, \phi)d\xi + \dots \\ & \frac{2\mu}{\pi(\kappa+1)} \int_0^\infty B_r^\oplus(\rho)G_{r\theta\theta}(r, -\alpha, \rho, \alpha) + B_\theta^\oplus(\rho)G_{\theta\theta\theta}(r, -\alpha, \rho, \alpha) \\ & + B_r^\ominus(\rho)G_{r\theta\theta}(r, -\alpha, \rho, -\alpha) + \dots \\ & B_\theta^\ominus(\rho)G_{\theta\theta\theta}(r, -\alpha, \rho, -\alpha)d\rho \quad \text{for } 0 \leq r \leq \infty. \end{aligned} \quad (\text{A.6})$$

These equations can then be discretised using the Gauss–Chebyshev quadratures, as described by Hills et al. (2013). We require the free surface dislocations to have a singular-bounded quadrature(denoted v for collocation points, u for integration points and X for weights), and the crack dislocations to have a bounded-singular quadrature(denoted t for collocation points, s for integration points and W for weights).

These points must be transformed in two different ways. The free surface points use a Mellin transform, given by $r = l \log \frac{2}{1-s}$, and $\xi = l \log \frac{2}{1-s}$. Whereas the crack points use a finite transform given by $r = \frac{2v}{l} - 1$, and $\rho = \frac{2u}{l} - 1$.

Finally, we can now write the discretised forms of the integral equations as:

$$\begin{aligned} & -K_{II}f_{r\theta}^I(\phi)t^{\lambda_I-1} - K_{III}f_{r\theta}^{II}(\phi)t^{\lambda_{III}-1} = \frac{2\mu}{\pi(\kappa+1)} \dots \\ & \left[\sum_{i=1}^n W(s_i)\varphi_r(s_i)G_{rr\theta}(t, \phi, s_i, \phi) + W(s_i)\varphi_\theta(s_i)G_{\theta r\theta}(t, \phi, s_i, \phi) + \dots \right. \\ & \sum_{i=1}^N X(u_i)\varphi_r^\oplus(u_i)G_{rr\theta}(t, \phi, u_i, \alpha) + X(u_i)\varphi_\theta^\oplus(u_i)G_{\theta r\theta}(t, \phi, u_i, \alpha) + \dots \\ & \left. X(u_i)\varphi_r^\ominus(u_i)G_{rr\theta}(t, \phi, u_i, -\alpha) + X(u_i)\varphi_\theta^\ominus(u_i)G_{\theta r\theta}(t, \phi, u_i, -\alpha) \right], \quad (\text{A.7}) \end{aligned}$$

$$\begin{aligned} & -K_{II}f_{\theta\theta}^I(\phi)t^{\lambda_I-1} - K_{III}f_{\theta\theta}^{II}(\phi)t^{\lambda_{III}-1} = \frac{2\mu}{\pi(\kappa+1)} \dots \\ & \left[\sum_{i=1}^n W(s_i)\varphi_r(s_i)G_{r\theta\theta}(t, \phi, s_i, \phi) + W(s_i)\varphi_\theta(s_i)G_{\theta\theta\theta}(t, \phi, s_i, \phi) + \dots \right. \\ & \sum_{i=1}^N X(u_i)\varphi_r^\oplus(u_i)G_{r\theta\theta}(t, \phi, u_i, \alpha) + X(u_i)\varphi_\theta^\oplus(u_i)G_{\theta\theta\theta}(t, \phi, u_i, \alpha) + \dots \\ & \left. X(u_i)\varphi_r^\ominus(u_i)G_{r\theta\theta}(t, \phi, u_i, -\alpha) + X(u_i)\varphi_\theta^\ominus(u_i)G_{\theta\theta\theta}(t, \phi, u_i, -\alpha) \right], \quad (\text{A.8}) \end{aligned}$$

$$\begin{aligned} 0 &= \frac{2\mu}{\pi(\kappa+1)} \left[\sum_{i=1}^n W(s_i)\varphi_r(s_i)G_{rr\theta}(v, \alpha, s_i, \phi) \right. \\ & + W(s_i)\varphi_\theta(s_i)G_{\theta r\theta}(v, \alpha, s_i, \phi) + \dots \\ & \sum_{i=1}^N X(u_i)\varphi_r^\oplus(u_i)G_{rr\theta}(v, \alpha, u_i, \alpha) + X(u_i)\varphi_\theta^\oplus(u_i)G_{\theta r\theta}(v, \alpha, u_i, \alpha) + \dots \\ & \left. X(u_i)\varphi_r^\ominus(u_i)G_{rr\theta}(v, \alpha, u_i, -\alpha) + X(u_i)\varphi_\theta^\ominus(u_i)G_{\theta r\theta}(v, \alpha, u_i, -\alpha) \right], \quad (\text{A.9}) \end{aligned}$$

$$\begin{aligned} 0 &= \frac{2\mu}{\pi(\kappa+1)} \left[\sum_{i=1}^n W(s_i)\varphi_r(s_i)G_{r\theta\theta}(v, \alpha, s_i, \phi) \right. \\ & + W(s_i)\varphi_\theta(s_i)G_{\theta\theta\theta}(v, \alpha, s_i, \phi) + \dots \\ & \sum_{i=1}^N X(u_i)\varphi_r^\oplus(u_i)G_{r\theta\theta}(v, \alpha, u_i, \alpha) + X(u_i)\varphi_\theta^\oplus(u_i)G_{\theta\theta\theta}(v, \alpha, u_i, \alpha) + \dots \\ & \left. X(u_i)\varphi_r^\ominus(u_i)G_{r\theta\theta}(v, \alpha, u_i, -\alpha) + X(u_i)\varphi_\theta^\ominus(u_i)G_{\theta\theta\theta}(v, \alpha, u_i, -\alpha) \right], \quad (\text{A.10}) \end{aligned}$$

$$0 = \frac{2\mu}{\pi(\kappa+1)} \left[\sum_{i=1}^n W(s_i)\varphi_r(s_i)G_{rr\theta}(v, -\alpha, s_i, \phi) \right.$$

$$\begin{aligned}
& + W(s_i)\varphi_\theta(s_i)G_{\theta r\theta}(v, -\alpha, s_i, \phi) + \dots \\
& \sum_{i=1}^N X(u_i)\varphi_r^\oplus(u_i)G_{rr\theta}(v, -\alpha, u_i, \alpha) + X(u_i)\varphi_\theta^\oplus(u_i)G_{\theta r\theta}(v, -\alpha, u_i, \alpha) + \dots \\
& \left. X(u_i)\varphi_r^\ominus(u_i)G_{rr\theta}(v, -\alpha, u_i, -\alpha) + X(u_i)\varphi_\theta^\ominus(u_i)G_{\theta r\theta}(v, -\alpha, u_i, -\alpha) \right], \quad (\text{A.11})
\end{aligned}$$

$$\begin{aligned}
0 = & \frac{2\mu}{\pi(\kappa+1)} \left[\sum_{i=1}^n W(s_i)\varphi_r(s_i)G_{r\theta\theta}(v, -\alpha, s_i, \phi) \right. \\
& + W(s_i)\varphi_\theta(s_i)G_{\theta\theta\theta}(v, -\alpha, s_i, \phi) + \dots \\
& \sum_{i=1}^N X(u_i)\varphi_r^\oplus(u_i)G_{rr\theta}(v, -\alpha, u_i, \alpha) + X(u_i)\varphi_\theta^\oplus(u_i)G_{\theta r\theta}(v, -\alpha, u_i, \alpha) + \dots \\
& \left. X(u_i)\varphi_r^\ominus(u_i)G_{rr\theta}(v, -\alpha, u_i, -\alpha) + X(u_i)\varphi_\theta^\ominus(u_i)G_{\theta r\theta}(v, -\alpha, u_i, -\alpha) \right]. \quad (\text{A.12})
\end{aligned}$$

The solution of this set of simultaneous equations will allow us to determine the dislocation densities along the crack faces and the free surfaces. This allows us to determine the state of stress in the wedge, and the crack tip stress intensity factors, in relationship to the wedge stress intensity factors.

Appendix B. Slip problem integral equations

The normal and shear tractions along the slip interface are given by

$$\sigma_{r\theta} = K_I f_{r\theta}^I(\theta) r^{\lambda_{II}-1} + K_{II} f_{r\theta}^{II}(\theta) r^{\lambda_{II}-1} + \dots \quad (\text{B.1})$$

$$\begin{aligned}
& \frac{2\mu}{\pi(\kappa+1)} \int_0^c B_r(\xi) G_{rr\theta}(r, \phi, \xi, \phi) d\xi \\
& + \frac{2\mu}{\pi(\kappa+1)} \int_0^\infty B_r^\oplus(\rho) G_{rr\theta}(r, \phi, \rho, \alpha) + \dots \\
& B_\theta^\oplus(\rho) G_{\theta r\theta}(r, \phi, \rho, \alpha) + B_r^\ominus(\rho) G_{rr\theta}(r, \phi, \rho, -\alpha) \\
& + B_\theta^\ominus(\rho) G_{\theta r\theta}(r, \phi, \rho, -\alpha) d\rho, \\
\sigma_{\theta\theta} = & K_I f_{\theta\theta}^I(\theta) r^{\lambda_{II}-1} + K_{II} f_{\theta\theta}^{II}(\theta) r^{\lambda_{II}-1} + \dots \quad (\text{B.2}) \\
& \frac{2\mu}{\pi(\kappa+1)} \int_0^c B_r(\xi) G_{r\theta\theta}(r, \phi, \xi, \phi) d\xi \\
& + \frac{2\mu}{\pi(\kappa+1)} \int_0^\infty B_r^\oplus(\rho) G_{r\theta\theta}(r, \phi, \rho, \alpha) + \dots \\
& B_\theta^\oplus(\rho) G_{\theta\theta\theta}(r, \phi, \rho, \alpha) + B_r^\ominus(\rho) G_{r\theta\theta}(r, \phi, \rho, -\alpha) \\
& + B_\theta^\ominus(\rho) G_{\theta\theta\theta}(r, \phi, \rho, -\alpha) d\rho,
\end{aligned}$$

throughout these the superscript \oplus or \ominus refers to distributions of dislocation along the positive and negative angle free surfaces respectively.

Now having these formulae for the tractions we can proceed exactly as described by Riddoch and Hills (2023a,b,c) to find the integral equation governing slip behaviour. However, unlike previously where this is the only integral equation for us to solve, we now have a further four integral equations associated with the free surfaces, and ensuring that these are free of traction. The five resulting integral equations are given by

$$0 = (f_c f_{\theta\theta}^I(\theta) + f_{r\theta}^I(\theta)) K_I r^{\lambda_{II}-1} + (f_c f_{\theta\theta}^{II}(\theta) + f_{r\theta}^{II}(\theta)) K_{II} r^{\lambda_{II}-1} + \dots \quad (\text{B.3})$$

$$\begin{aligned}
& \int_0^c \bar{B}(\xi) [f_c G_{r\theta\theta}(r, \phi, \xi, \phi) + G_{rr\theta}(r, \phi, \xi, \phi)] d\xi \\
& + \int_0^\infty f_c [B_r^\oplus(\rho) G_{rr\theta}(r, \phi, \rho, \alpha) + \dots \\
& B_\theta^\oplus(\rho) G_{\theta\theta\theta}(r, \phi, \rho, \alpha) + B_r^\ominus(\rho) G_{r\theta\theta}(r, \phi, \rho, \alpha) + B_\theta^\ominus(\rho) G_{\theta\theta\theta}(r, \phi, \rho, \alpha)] \\
& + B_r^\oplus(\rho) G_{rr\theta}(r, \phi, \rho, \alpha) + \dots \\
& B_\theta^\oplus(\rho) G_{\theta r\theta}(r, \phi, \rho, \alpha) + B_r^\ominus(\rho) G_{rr\theta}(r, \phi, \rho, \alpha) \\
& + B_\theta^\ominus(\rho) G_{\theta r\theta}(r, \phi, \rho, \alpha) d\rho \quad \text{for } 0 \leq r \leq c,
\end{aligned}$$

$$\begin{aligned}
0 = & \int_0^c \bar{B}(\xi) G_{rr\theta}(r, \alpha, \xi, \phi) d\xi + \int_0^\infty B_r^\oplus(\rho) G_{rr\theta}(r, \alpha, \rho, \alpha) + \dots \quad (\text{B.4}) \\
& B_\theta^\oplus(\rho) G_{\theta r\theta}(r, \alpha, \rho, \alpha) + B_r^\ominus(\rho) G_{rr\theta}(r, \alpha, \rho, -\alpha) + B_\theta^\ominus(\rho) G_{\theta r\theta}(r, \alpha, \rho, -\alpha) d\rho \\
& \text{for } 0 \leq r \leq \infty.
\end{aligned}$$

$$\begin{aligned}
0 = & \int_0^c \bar{B}(\xi) G_{r\theta\theta}(r, \alpha, \xi, \phi) d\xi + \int_0^\infty B_r^\oplus(\rho) G_{r\theta\theta}(r, \alpha, \rho, \alpha) + \dots \quad (\text{B.5}) \\
& B_\theta^\oplus(\rho) G_{\theta\theta\theta}(r, \alpha, \rho, \alpha) + B_r^\ominus(\rho) G_{r\theta\theta}(r, \alpha, \rho, -\alpha) + B_\theta^\ominus(\rho) G_{\theta\theta\theta}(r, \alpha, \rho, -\alpha) d\rho \\
& \text{for } 0 \leq r \leq \infty.
\end{aligned}$$

$$\begin{aligned}
0 = & \int_0^c \bar{B}(\xi) G_{rr\theta}(r, -\alpha, \xi, \phi) d\xi + \int_0^\infty B_r^\oplus(\rho) G_{rr\theta}(r, -\alpha, \rho, \alpha) + \dots \quad (\text{B.6}) \\
& B_\theta^\oplus(\rho) G_{\theta r\theta}(r, -\alpha, \rho, \alpha) + B_r^\ominus(\rho) G_{rr\theta}(r, -\alpha, \rho, -\alpha) \\
& + B_\theta^\ominus(\rho) G_{\theta r\theta}(r, -\alpha, \rho, -\alpha) d\rho \quad \text{for } 0 \leq r \leq \infty.
\end{aligned}$$

$$\begin{aligned}
0 = & \int_0^c \bar{B}(\xi) G_{r\theta\theta}(r, -\alpha, \xi, \phi) d\xi + \int_0^\infty B_r^\oplus(\rho) G_{r\theta\theta}(r, -\alpha, \rho, \alpha) + \dots \quad (\text{B.7}) \\
& B_\theta^\oplus(\rho) G_{\theta\theta\theta}(r, -\alpha, \rho, \alpha) + B_r^\ominus(\rho) G_{r\theta\theta}(r, -\alpha, \rho, -\alpha) \\
& + B_\theta^\ominus(\rho) G_{\theta\theta\theta}(r, -\alpha, \rho, -\alpha) d\rho \quad \text{for } 0 \leq r \leq \infty.
\end{aligned}$$

These integral equations now must be discretised. We will use exactly the same Mellin transform for the free surface points as we did for the single crack problem, given by $r = c \log \frac{2}{1-t}$, for the collocation points and $\xi = c \log \frac{2}{1-s}$, for the integration points. However, the points on the slip interface use a different quadrature to that used by those on the crack faces. Whereas the crack face tractions used the bounded-singular quadrature, the slip points will use a bounded-bounded quadrature as discussed by Riddoch and Hills (2023a,b,c).

For the sake of clarity we will denote the collocation points by p , the integration points by q , and the weights by Y . The transformation is then the same linear transformation given by $r = \frac{2p}{c} - 1$, and $\xi = \frac{2q}{c} - 1$. Therefore we can discretise these equations by

$$\begin{aligned}
0 = & (f_c f_{\theta\theta}^I(\theta) + f_{r\theta}^I(\theta)) K_I p^{\lambda_{II}-1} + (f_c f_{\theta\theta}^{II}(\theta) + f_{r\theta}^{II}(\theta)) K_{II} p^{\lambda_{II}-1} + \dots \\
& \sum_{i=1}^n Y(q_i) \bar{\varphi}(q_i) [f_c G_{r\theta\theta}(p, \phi, q_i, \phi) + G_{rr\theta}(p, \phi, q_i, \phi)] \dots \\
& + \sum_{j=1}^N f_c [W(s_j) \varphi_r^\oplus(s_j) G_{r\theta\theta}(p, \phi, s_j, \alpha) \\
& + W(s_j) \varphi_\theta^\oplus(s_j) G_{\theta\theta\theta}(p, \phi, s_j, \alpha) + \dots \quad (\text{B.8}) \\
& W(s_j) \varphi_r^\ominus(s_j) G_{r\theta\theta}(p, \phi, s_j, \alpha) + W(s_j) \varphi_\theta^\ominus(s_j) G_{\theta\theta\theta}(p, \phi, s_j, \alpha)] \\
& + W(s_j) \varphi_r^\oplus(s_j) G_{rr\theta}(p, \phi, s_j, \alpha) + \dots \\
& W(s_j) \varphi_\theta^\oplus(s_j) G_{\theta r\theta}(p, \phi, s_j, \alpha) + W(s_j) \varphi_r^\ominus(s_j) G_{rr\theta}(p, \phi, s_j, \alpha) \\
& + W(s_j) \varphi_\theta^\ominus(s_j) G_{\theta r\theta}(p, \phi, s_j, \alpha),
\end{aligned}$$

$$\begin{aligned}
0 = & \sum_{i=1}^n Y(q_i) \bar{\varphi}(q_i) G_{rr\theta}(t, \alpha, s_i, \phi) + \sum_{i=1}^N W(s_i) \varphi_r^\oplus(s_i) G_{rr\theta}(t, \alpha, s_i, \alpha) + \dots \quad (\text{B.9}) \\
& W(s_i) \varphi_\theta^\oplus(s_i) G_{\theta r\theta}(t, \alpha, s_i, \alpha) + W(s_i) \varphi_r^\ominus(s_i) G_{rr\theta}(t, \alpha, s_i, -\alpha) \\
& + W(s_i) \varphi_\theta^\ominus(s_i) G_{\theta r\theta}(t, \alpha, s_i, -\alpha),
\end{aligned}$$

$$\begin{aligned}
0 = & \sum_{i=1}^n Y(q_i) \bar{\varphi}(q_i) G_{r\theta\theta}(t, \alpha, q_i, \phi) + \sum_{i=1}^N W(s_i) \varphi_r^\oplus(s_i) G_{r\theta\theta}(t, \alpha, s_i, \alpha) + \dots \quad (\text{B.10}) \\
& W(s_i) \varphi_\theta^\oplus(s_i) G_{\theta\theta\theta}(t, \alpha, s_i, \alpha) + W(s_i) \varphi_r^\ominus(s_i) G_{r\theta\theta}(t, \alpha, s_i, -\alpha) \\
& + W(s_i) \varphi_\theta^\ominus(s_i) G_{\theta\theta\theta}(t, \alpha, s_i, -\alpha),
\end{aligned}$$

$$\begin{aligned}
0 = & \sum_{i=1}^n Y(q_i) \bar{\varphi}(q_i) G_{rr\theta}(t, -\alpha, q_i, \phi) + \sum_{i=1}^N W(s_i) \varphi_r^\oplus(s_i) G_{rr\theta}(t, -\alpha, s_i, \alpha) + \dots \quad (\text{B.11}) \\
& W(s_i) \varphi_\theta^\oplus(s_i) G_{\theta r\theta}(t, -\alpha, s_i, \alpha) + W(s_i) \varphi_r^\ominus(s_i) G_{rr\theta}(t, -\alpha, s_i, -\alpha) \\
& + W(s_i) \varphi_\theta^\ominus(s_i) G_{\theta r\theta}(t, -\alpha, s_i, -\alpha),
\end{aligned}$$

$$0 = \sum_{i=1}^n Y(q_i) \bar{\varphi}(q_i) G_{r\theta\theta}(t, -\alpha, q_i, \phi) + \sum_{i=1}^N W(s_i) \varphi_r^{\oplus}(s_i) G_{r\theta\theta}(t, -\alpha, s_i, \alpha) + \dots \quad (\text{B.12})$$

$$W(s_i) \varphi_{\theta}^{\oplus}(s_i) G_{\theta\theta\theta}(t, -\alpha, s_i, \alpha) + W(s_i) \varphi_r^{\ominus}(s_i) G_{r\theta\theta}(t, -\alpha, s_i, -\alpha) + W(s_i) \varphi_{\theta}^{\ominus}(s_i) G_{\theta\theta\theta}(t, -\alpha, s_i, -\alpha).$$

The solution of this set of equations, and the attendant determination of the true size of the slip zone will allow us to determine the state of stress in a slipping complete contact.

Appendix C. Two crack integral equations

As with the single crack problem these two pairs of distributions will have different integration ranges, and again we denote the free surface dislocations using the superscripts \oplus, \ominus . This leads us to a set of eight simultaneous singular integral equations, given by:

$$\begin{aligned} \frac{2\mu}{\pi(\kappa+1)} \left[\int_0^{l_1} B_r^1(\rho) G_{rr\theta}(r, \phi_1, \rho, \phi_1) + B_{\theta}^1(\rho) G_{\theta r\theta}(r, \phi_1, \rho, \phi_1) d\rho + \dots \right. \\ \int_0^{l_2} B_r^2(\rho) G_{rr\theta}(r, \phi_1, \rho, \phi_2) + B_{\theta}^2(\rho) G_{\theta r\theta}(r, \phi_1, \rho, \phi_2) d\rho \\ \left. + \int_0^{\infty} B_r^{\oplus}(\rho) G_{rr\theta}(r, \phi_1, \rho, \alpha) + \dots \right. \\ \left. B_{\theta}^{\oplus}(\rho) G_{\theta r\theta}(r, \phi_1, \rho, \alpha) + B_r^{\ominus}(\rho) G_{rr\theta}(r, \phi_1, \rho, -\alpha) \right. \\ \left. + B_{\theta}^{\ominus}(\rho) G_{\theta r\theta}(r, \phi_1, \rho, -\alpha) d\rho \right] = \dots \\ - K_I f_{r\theta}^I(\phi_1) r^{\lambda_I-1} - K_{II} f_{r\theta}^{II}(\phi_1) r^{\lambda_{II}-1}. \quad (\text{C.1}) \end{aligned}$$

$$\begin{aligned} \frac{2\mu}{\pi(\kappa+1)} \left[\int_0^{l_1} B_r^1(\rho) G_{r\theta\theta}(r, \phi_1, \rho, \phi_1) + B_{\theta}^1(\rho) G_{\theta\theta\theta}(r, \phi_1, \rho, \phi_1) d\rho + \dots \right. \\ \int_0^{l_2} B_r^2(\rho) G_{r\theta\theta}(r, \phi_1, \rho, \phi_2) + B_{\theta}^2(\rho) G_{\theta\theta\theta}(r, \phi_1, \rho, \phi_2) d\rho \\ \left. + \int_0^{\infty} B_r^{\oplus}(\rho) G_{r\theta\theta}(r, \phi_1, \rho, \alpha) + \dots \right. \\ \left. B_{\theta}^{\oplus}(\rho) G_{\theta\theta\theta}(r, \phi_1, \rho, \alpha) + B_r^{\ominus}(\rho) G_{r\theta\theta}(r, \phi_1, \rho, -\alpha) \right. \\ \left. + B_{\theta}^{\ominus}(\rho) G_{\theta\theta\theta}(r, \phi_1, \rho, -\alpha) d\rho \right] = \dots \\ - K_I f_{\theta\theta}^I(\phi_1) r^{\lambda_I-1} - K_{II} f_{\theta\theta}^{II}(\phi_1) r^{\lambda_{II}-1}. \quad (\text{C.2}) \end{aligned}$$

$$\begin{aligned} \frac{2\mu}{\pi(\kappa+1)} \left[\int_0^{l_1} B_r^1(\rho) G_{rr\theta}(r, \phi_2, \rho, \phi_1) + B_{\theta}^1(\rho) G_{\theta r\theta}(r, \phi_2, \rho, \phi_1) d\rho + \dots \right. \\ \int_0^{l_2} B_r^2(\rho) G_{rr\theta}(r, \phi_2, \rho, \phi_2) + B_{\theta}^2(\rho) G_{\theta r\theta}(r, \phi_2, \rho, \phi_2) d\rho \\ \left. + \int_0^{\infty} B_r^{\oplus}(\rho) G_{rr\theta}(r, \phi_2, \rho, \alpha) + \dots \right. \\ \left. B_{\theta}^{\oplus}(\rho) G_{\theta r\theta}(r, \phi_2, \rho, \alpha) + B_r^{\ominus}(\rho) G_{rr\theta}(r, \phi_2, \rho, -\alpha) \right. \\ \left. + B_{\theta}^{\ominus}(\rho) G_{\theta r\theta}(r, \phi_2, \rho, -\alpha) d\rho \right] = \dots \\ - K_I f_{r\theta}^I(\phi_2) r^{\lambda_I-1} - K_{II} f_{r\theta}^{II}(\phi_2) r^{\lambda_{II}-1}. \quad (\text{C.3}) \end{aligned}$$

$$\begin{aligned} \frac{2\mu}{\pi(\kappa+1)} \left[\int_0^{l_1} B_r^1(\rho) G_{r\theta\theta}(r, \phi_2, \rho, \phi_1) + B_{\theta}^1(\rho) G_{\theta\theta\theta}(r, \phi_2, \rho, \phi_1) d\rho + \dots \right. \\ \int_0^{l_2} B_r^2(\rho) G_{r\theta\theta}(r, \phi_2, \rho, \phi_2) + B_{\theta}^2(\rho) G_{\theta\theta\theta}(r, \phi_2, \rho, \phi_2) d\rho \\ \left. + \int_0^{\infty} B_r^{\oplus}(\rho) G_{r\theta\theta}(r, \phi_2, \rho, \alpha) + \dots \right. \\ \left. B_{\theta}^{\oplus}(\rho) G_{\theta\theta\theta}(r, \phi_2, \rho, \alpha) + B_r^{\ominus}(\rho) G_{r\theta\theta}(r, \phi_2, \rho, -\alpha) \right. \\ \left. + B_{\theta}^{\ominus}(\rho) G_{\theta\theta\theta}(r, \phi_2, \rho, -\alpha) d\rho \right] = \dots \\ - K_I f_{\theta\theta}^I(\phi_2) r^{\lambda_I-1} - K_{II} f_{\theta\theta}^{II}(\phi_2) r^{\lambda_{II}-1}. \quad (\text{C.4}) \end{aligned}$$

$$\begin{aligned} \frac{2\mu}{\pi(\kappa+1)} \left[\int_0^{l_1} B_r^1(\rho) G_{rr\theta}(r, \alpha, \rho, \phi_1) + B_{\theta}^1(\rho) G_{\theta r\theta}(r, \alpha, \rho, \phi_1) d\rho + \dots \right. \\ \int_0^{l_2} B_r^2(\rho) G_{rr\theta}(r, \alpha, \rho, \phi_2) + B_{\theta}^2(\rho) G_{\theta r\theta}(r, \alpha, \rho, \phi_2) d\rho \\ \left. + \int_0^{\infty} B_r^{\oplus}(\rho) G_{rr\theta}(r, \alpha, \rho, \alpha) + \dots \right. \\ \left. B_{\theta}^{\oplus}(\rho) G_{\theta r\theta}(r, \alpha, \rho, \alpha) + B_r^{\ominus}(\rho) G_{rr\theta}(r, \alpha, \rho, -\alpha) \right. \\ \left. + B_{\theta}^{\ominus}(\rho) G_{\theta r\theta}(r, \alpha, \rho, -\alpha) d\rho \right] = 0. \quad (\text{C.5}) \end{aligned}$$

$$\begin{aligned} \frac{2\mu}{\pi(\kappa+1)} \left[\int_0^{l_1} B_r^1(\rho) G_{r\theta\theta}(r, \alpha, \rho, \phi_1) + B_{\theta}^1(\rho) G_{\theta\theta\theta}(r, \alpha, \rho, \phi_1) d\rho + \dots \right. \\ \int_0^{l_2} B_r^2(\rho) G_{r\theta\theta}(r, \alpha, \rho, \phi_2) + B_{\theta}^2(\rho) G_{\theta\theta\theta}(r, \alpha, \rho, \phi_2) d\rho \\ \left. + \int_0^{\infty} B_r^{\oplus}(\rho) G_{r\theta\theta}(r, \alpha, \rho, \alpha) + \dots \right. \\ \left. B_{\theta}^{\oplus}(\rho) G_{\theta\theta\theta}(r, \alpha, \rho, \alpha) + B_r^{\ominus}(\rho) G_{r\theta\theta}(r, \alpha, \rho, -\alpha) \right. \\ \left. + B_{\theta}^{\ominus}(\rho) G_{\theta\theta\theta}(r, \alpha, \rho, -\alpha) d\rho \right] = 0. \quad (\text{C.6}) \end{aligned}$$

$$\begin{aligned} \frac{2\mu}{\pi(\kappa+1)} \left[\int_0^{l_1} B_r^1(\rho) G_{rr\theta}(r, -\alpha, \rho, \phi_1) + B_{\theta}^1(\rho) G_{\theta r\theta}(r, -\alpha, \rho, \phi_1) d\rho + \dots \right. \\ \int_0^{l_2} B_r^2(\rho) G_{rr\theta}(r, -\alpha, \rho, \phi_2) + B_{\theta}^2(\rho) G_{\theta r\theta}(r, -\alpha, \rho, \phi_2) d\rho \\ \left. + \int_0^{\infty} B_r^{\oplus}(\rho) G_{rr\theta}(r, -\alpha, \rho, \alpha) + \dots \right. \\ \left. B_{\theta}^{\oplus}(\rho) G_{\theta r\theta}(r, -\alpha, \rho, \alpha) + B_r^{\ominus}(\rho) G_{rr\theta}(r, -\alpha, \rho, -\alpha) \right. \\ \left. + B_{\theta}^{\ominus}(\rho) G_{\theta r\theta}(r, -\alpha, \rho, -\alpha) d\rho \right] = 0, \quad (\text{C.7}) \end{aligned}$$

$$\begin{aligned} \frac{2\mu}{\pi(\kappa+1)} \left[\int_0^{l_1} B_r^1(\rho) G_{r\theta\theta}(r, -\alpha, \rho, \phi_1) + B_{\theta}^1(\rho) G_{\theta\theta\theta}(r, -\alpha, \rho, \phi_1) d\rho + \dots \right. \\ \int_0^{l_2} B_r^2(\rho) G_{r\theta\theta}(r, -\alpha, \rho, \phi_2) + B_{\theta}^2(\rho) G_{\theta\theta\theta}(r, -\alpha, \rho, \phi_2) d\rho \\ \left. + \int_0^{\infty} B_r^{\oplus}(\rho) G_{r\theta\theta}(r, -\alpha, \rho, \alpha) + \dots \right. \\ \left. B_{\theta}^{\oplus}(\rho) G_{\theta\theta\theta}(r, -\alpha, \rho, \alpha) + B_r^{\ominus}(\rho) G_{r\theta\theta}(r, -\alpha, \rho, -\alpha) \right. \\ \left. + B_{\theta}^{\ominus}(\rho) G_{\theta\theta\theta}(r, -\alpha, \rho, -\alpha) d\rho \right] = 0. \quad (\text{C.8}) \end{aligned}$$

Once again we will discretise these equations using the Gauss–Chebyshev quadratures. This is done in exactly the same way as for the single crack problem, the only difference being the introduction of the factor $l_R := \frac{l_1}{l_2}$. So, as before the points must be transformed in two different ways. The free surface points use a Mellin transform, given by $r = l \log \frac{2}{1-t}$, and $\xi = l \log \frac{2}{1-s}$. Whereas the crack points use a finite transform given by $r = \frac{2v}{l_1} - 1$, and $\rho = \frac{2u}{l_1} - 1$. This therefore allows us to discretise our eight integral equations into eight sums, given by:

$$\begin{aligned} \frac{2\mu}{\pi(\kappa+1)} \left[\sum_{i=1}^n W(s_i) \varphi_r^1(s_i) G_{rr\theta}(t, \phi_1, s_i, \phi_1) \right. \\ \left. + W(s_i) \varphi_{\theta}^1(s_i) G_{\theta r\theta}(t, \phi_1, s_i, \phi_1) + \dots \right. \\ \left. W(s_i) \varphi_r^2(s_i) G_{rr\theta}(t, \phi_1, l_R s_i, \phi_2) + W(s_i) \varphi_{\theta}^2(s_i) G_{\theta r\theta}(t, \phi_1, l_R s_i, \phi_2) + \dots \right. \\ \sum_{i=1}^N X(u_i) \varphi_r^{\oplus}(u_i) G_{rr\theta}(t, \phi_1, u_i, \alpha) + X(u_i) \varphi_{\theta}^{\oplus}(u_i) G_{\theta r\theta}(t, \phi_1, u_i, \alpha) + \dots \\ \left. X(u_i) \varphi_r^{\ominus}(u_i) G_{rr\theta}(t, \phi_1, u_i, -\alpha) \right. \\ \left. + X(u_i) \varphi_{\theta}^{\ominus}(u_i) G_{\theta r\theta}(t, \phi_1, u_i, -\alpha) \right] = \dots \\ - K_I f_{r\theta}^I(\phi_1) t^{\lambda_I-1} - K_{II} f_{r\theta}^{II}(\phi_1) t^{\lambda_{II}-1}, \quad (\text{C.9}) \end{aligned}$$

$$\begin{aligned}
& \frac{2\mu}{\pi(\kappa+1)} \left[\sum_{i=1}^n W(s_i) \varphi_r^1(s_i) G_{r\theta\theta}(t, \phi_1, s_i, \phi_1) \right. \\
& + W(s_i) \varphi_\theta^1(s_i) G_{\theta\theta\theta}(t, \phi_1, s_i, \phi_1) + \dots \\
& W(s_i) \varphi_r^2(s_i) G_{r\theta\theta}(t, \phi_1, l_R s_i, \phi_2) \\
& + W(s_i) \varphi_\theta^2(s_i) G_{\theta\theta\theta}(t, \phi_1, l_R s_i, \phi_2) + \dots \\
& \sum_{i=1}^N X(u_i) \varphi_r^\oplus(u_i) G_{r\theta\theta}(t, \phi_1, u_i, \alpha) + X(u_i) \varphi_\theta^\oplus(u_i) G_{\theta\theta\theta}(t, \phi_1, u_i, \alpha) + \dots \\
& X(u_i) \varphi_r^\ominus(u_i) G_{r\theta\theta}(t, \phi_1, u_i, -\alpha) \\
& \left. + X(u_i) \varphi_\theta^\ominus(u_i) G_{\theta\theta\theta}(t, \phi_1, u_i, -\alpha) \right] = \dots \\
& - K_I f_{\theta\theta}^I(\phi_1) l^{\lambda_I-1} - K_{II} f_{\theta\theta}^{II}(\phi_1) l^{\lambda_{II}-1}, \quad (C.10)
\end{aligned}$$

$$\begin{aligned}
& \frac{2\mu}{\pi(\kappa+1)} \left[\sum_{i=1}^n W(s_i) \varphi_r^1(s_i) G_{rr\theta}(l_R t, \phi_1, s_i, \phi_1) \right. \\
& + W(s_i) \varphi_\theta^1(s_i) G_{\theta r\theta}(l_R t, \phi_1, s_i, \phi_1) + \dots \\
& W(s_i) \varphi_r^2(s_i) G_{rr\theta}(l_R t, \phi_1, l_R s_i, \phi_2) \\
& + W(s_i) \varphi_\theta^2(s_i) G_{\theta r\theta}(l_R t, \phi_1, l_R s_i, \phi_2) + \dots \\
& \sum_{i=1}^N X(u_i) \varphi_r^\oplus(u_i) G_{rr\theta}(l_R t, \phi_1, u_i, \alpha) \\
& + X(u_i) \varphi_\theta^\oplus(u_i) G_{\theta r\theta}(l_R t, \phi_1, u_i, \alpha) + \dots \\
& X(u_i) \varphi_r^\ominus(u_i) G_{rr\theta}(l_R t, \phi_1, u_i, -\alpha) \\
& \left. + X(u_i) \varphi_\theta^\ominus(u_i) G_{\theta r\theta}(l_R t, \phi_1, u_i, -\alpha) \right] = \dots \\
& - K_I f_{rr}^I(\phi_1) (l_R t)^{\lambda_I-1} - K_{II} f_{rr}^{II}(\phi_1) (l_R t)^{\lambda_{II}-1}, \quad (C.11)
\end{aligned}$$

$$\begin{aligned}
& \frac{2\mu}{\pi(\kappa+1)} \left[\sum_{i=1}^n W(s_i) \varphi_r^1(s_i) G_{r\theta\theta}(l_R t, \phi_1, s_i, \phi_1) \right. \\
& + W(s_i) \varphi_\theta^1(s_i) G_{\theta\theta\theta}(l_R t, \phi_1, s_i, \phi_1) + \dots \\
& W(s_i) \varphi_r^2(s_i) G_{r\theta\theta}(l_R t, \phi_1, l_R s_i, \phi_2) \\
& + W(s_i) \varphi_\theta^2(s_i) G_{\theta\theta\theta}(l_R t, \phi_1, l_R s_i, \phi_2) + \dots \\
& \sum_{i=1}^N X(u_i) \varphi_r^\oplus(u_i) G_{r\theta\theta}(l_R t, \phi_1, u_i, \alpha) \\
& + X(u_i) \varphi_\theta^\oplus(u_i) G_{\theta\theta\theta}(l_R t, \phi_1, u_i, \alpha) + \dots \\
& X(u_i) \varphi_r^\ominus(u_i) G_{r\theta\theta}(l_R t, \phi_1, u_i, -\alpha) \\
& \left. + X(u_i) \varphi_\theta^\ominus(u_i) G_{\theta\theta\theta}(l_R t, \phi_1, u_i, -\alpha) \right] = \dots \\
& - K_I f_{\theta\theta}^I(\phi_1) (l_R t)^{\lambda_I-1} - K_{II} f_{\theta\theta}^{II}(\phi_1) (l_R t)^{\lambda_{II}-1}, \quad (C.12)
\end{aligned}$$

$$\begin{aligned}
& \frac{2\mu}{\pi(\kappa+1)} \left[\sum_{i=1}^n W(s_i) \varphi_r^1(s_i) G_{rr\theta}(v, \phi_1, s_i, \phi_1) \right. \\
& + W(s_i) \varphi_\theta^1(s_i) G_{\theta r\theta}(v, \phi_1, s_i, \phi_1) + \dots \\
& W(s_i) \varphi_r^2(s_i) G_{rr\theta}(v, \phi_1, l_R s_i, \phi_2) \\
& + W(s_i) \varphi_\theta^2(s_i) G_{\theta r\theta}(v, \phi_1, l_R s_i, \phi_2) + \dots \\
& \sum_{i=1}^N X(u_i) \varphi_r^\oplus(u_i) G_{rr\theta}(v, \phi_1, u_i, \alpha) \\
& + X(u_i) \varphi_\theta^\oplus(u_i) G_{\theta r\theta}(v, \phi_1, u_i, \alpha) + \dots \\
& X(u_i) \varphi_r^\ominus(u_i) G_{rr\theta}(v, \phi_1, u_i, -\alpha) \\
& \left. + X(u_i) \varphi_\theta^\ominus(u_i) G_{\theta r\theta}(v, \phi_1, u_i, -\alpha) \right] = 0, \quad (C.13)
\end{aligned}$$

$$\begin{aligned}
& \frac{2\mu}{\pi(\kappa+1)} \left[\sum_{i=1}^n W(s_i) \varphi_r^1(s_i) G_{r\theta\theta}(v, \phi_1, s_i, \phi_1) \right. \\
& + W(s_i) \varphi_\theta^1(s_i) G_{\theta\theta\theta}(v, \phi_1, s_i, \phi_1) + \dots \\
& W(s_i) \varphi_r^2(s_i) G_{r\theta\theta}(v, \phi_1, l_R s_i, \phi_2) + W(s_i) \varphi_\theta^2(s_i) G_{\theta\theta\theta}(v, \phi_1, l_R s_i, \phi_2) + \dots
\end{aligned}$$

$$\begin{aligned}
& \sum_{i=1}^N X(u_i) \varphi_r^\oplus(u_i) G_{r\theta\theta}(v, \phi_1, u_i, \alpha) + X(u_i) \varphi_\theta^\oplus(u_i) G_{\theta\theta\theta}(v, \phi_1, u_i, \alpha) + \dots \\
& X(u_i) \varphi_r^\ominus(u_i) G_{r\theta\theta}(v, \phi_1, u_i, -\alpha) \\
& \left. + X(u_i) \varphi_\theta^\ominus(u_i) G_{\theta\theta\theta}(v, \phi_1, u_i, -\alpha) \right] = 0, \quad (C.14)
\end{aligned}$$

$$\begin{aligned}
& \frac{2\mu}{\pi(\kappa+1)} \left[\sum_{i=1}^n W(s_i) \varphi_r^1(s_i) G_{rr\theta}(v, \phi_1, s_i, \phi_1) \right. \\
& + W(s_i) \varphi_\theta^1(s_i) G_{\theta r\theta}(v, \phi_1, s_i, \phi_1) + \dots \\
& W(s_i) \varphi_r^2(s_i) G_{rr\theta}(v, \phi_1, l_R s_i, \phi_2) + W(s_i) \varphi_\theta^2(s_i) G_{\theta r\theta}(v, \phi_1, l_R s_i, \phi_2) + \dots \\
& \sum_{i=1}^N X(u_i) \varphi_r^\oplus(u_i) G_{rr\theta}(v, \phi_1, u_i, \alpha) + X(u_i) \varphi_\theta^\oplus(u_i) G_{\theta r\theta}(v, \phi_1, u_i, \alpha) + \dots \\
& X(u_i) \varphi_r^\ominus(u_i) G_{rr\theta}(v, \phi_1, u_i, -\alpha) \\
& \left. + X(u_i) \varphi_\theta^\ominus(u_i) G_{\theta r\theta}(v, \phi_1, u_i, -\alpha) \right] = 0, \quad (C.15)
\end{aligned}$$

$$\begin{aligned}
& \frac{2\mu}{\pi(\kappa+1)} \left[\sum_{i=1}^n W(s_i) \varphi_r^1(s_i) G_{r\theta\theta}(v, \phi_1, s_i, \phi_1) \right. \\
& + W(s_i) \varphi_\theta^1(s_i) G_{\theta\theta\theta}(v, \phi_1, s_i, \phi_1) + \dots \\
& W(s_i) \varphi_r^2(s_i) G_{r\theta\theta}(v, \phi_1, l_R s_i, \phi_2) + W(s_i) \varphi_\theta^2(s_i) G_{\theta\theta\theta}(v, \phi_1, l_R s_i, \phi_2) + \dots \\
& \sum_{i=1}^N X(u_i) \varphi_r^\oplus(u_i) G_{r\theta\theta}(v, \phi_1, u_i, \alpha) + X(u_i) \varphi_\theta^\oplus(u_i) G_{\theta\theta\theta}(v, \phi_1, u_i, \alpha) + \dots \\
& X(u_i) \varphi_r^\ominus(u_i) G_{r\theta\theta}(v, \phi_1, u_i, -\alpha) \\
& \left. + X(u_i) \varphi_\theta^\ominus(u_i) G_{\theta\theta\theta}(v, \phi_1, u_i, -\alpha) \right] = 0.
\end{aligned}$$

References

- Churchman, C., Hills, D., 2006a. The edge dislocation in a three-quarter plane. Part II: Application to an edge crack. *Eur. J. Mech. A Solids* 25 (3), 389–396.
- Churchman, C., Hills, D., 2006b. Slip zone length at the edge of a complete contact. *Int. J. Solids Struct.* 43 (7–8), 2037–2049.
- Churchman, C., Korsunsky, A., Hills, D., 2006. The edge dislocation in a three-quarter plane. Part I: Influence functions. *Eur. J. Mech. A Solids* 25 (1), 42–50.
- Cottrell, A.H., Seeger, A., Amorós, J., 1956. Dislocations in crystals. In: *Deformation and Flow of Solids/Verformung und Fließen des Festkörpers*. Springer, pp. 33–52.
- Erdogan, F., Gupta, G.D., Cook, T., 1973. Numerical solution of singular integral equations. In: *Methods of Analysis and Solutions of Crack Problems*. Springer, pp. 368–425.
- Hecker, M., Romanov, A., 1992. The stress fields of an edge dislocation near a wedge-shaped boundary. *Phys. Status Solidi A* 130 (1), 91–101.
- Hecker, M., Romanov, A., 1993. The stress fields of edge dislocations near wedge-shaped boundaries and bonded wedges. In: *Fundamental Aspects of Dislocation Interactions*. Elsevier, pp. 411–414.
- Hills, D., Dini, D., 2004. What level of friction guarantees adhesion in a complete contact? *J. Strain Anal. Eng. Des.* 39 (5), 549–551.
- Hills, D.A., Dini, D., 2011. Characteristics of the process zone at sharp notch roots. *Int. J. Solids Struct.* 48 (14–15), 2177–2183.
- Hills, D.A., Kelly, P.A., Dai, D.N., Korsunsky, A.M., 2013. In: Gladwell, G.M.L. (Ed.), *Solution of Crack Problems: The Distributed Dislocation Technique*, Vol. 44. Springer Science & Business Media.
- Riddoch, D.J., Hills, D.A., 2020. Necessary conditions for near-edge stick of complete contacts. *J. Strain Anal. Eng. Des.* 55 (5–6), 172–180.
- Riddoch, D.J., Hills, D.A., 2023a. Dislocations in an arbitrary angle wedge. Part II: Cracks in the wedge. *J. Strain Anal. Eng. Des.* (in press).
- Riddoch, D.J., Hills, D.A., 2023b. Dislocations in an arbitrary angle wedge. Part I: The dislocation kernel. *J. Strain Anal. Eng. Des.* (in press).
- Riddoch, D.J., Hills, D.A., 2023c. Slip at the edge of complete contacts. *Proc. Inst. Mech. Eng. C* 09544062221142695.
- Williams, M., 1952. Stress singularities resulting from various boundary conditions in angular corners of plates in extension. *J. Appl. Mech.* 19 (4), 526–528.
- Yingzhi, L., Hills, D., 1990. Stress intensity factor solutions for kinked surface cracks. *J. Strain Anal. Eng. Des.* 25 (1), 21–27.